

# Using atmospheric trace gas vertical profiles to evaluate model fluxes: a case-study of Arctic-CAP observations and GEOS simulations for the ABoVE domain

5 Colm Sweeney<sup>1</sup>, Abhishek Chatterjee<sup>2,3</sup>, Sonja Wolter<sup>4,1</sup>, Kathryn McKain<sup>4,1</sup>, Robert Bogue<sup>5\*</sup>, Tim Newberger<sup>4,1</sup>, Lei Hu<sup>4,1</sup>, Lesley Ott<sup>3</sup>, Benjamin Poulter<sup>3</sup>, Luke Schiferl<sup>6</sup>, Brad Weir<sup>2,3</sup>, Zhen Zhang<sup>7</sup>, Charles E. Miller<sup>5</sup>

<sup>1</sup>NOAA Earth System Research Laboratory, Boulder, CO, USA

<sup>2</sup>Universities Space Research Association, Columbia, MD, USA

<sup>3</sup>NASA Goddard Space Flight Center, Greenbelt MD, USA

10 <sup>4</sup>CIRES, University of Colorado, Boulder, CO, USA

<sup>5</sup>Jet Propulsion Laboratory, California Institute of Technology, Pasadena CA, USA

<sup>6</sup>LDEO, Columbia University, New York, NY, USA

<sup>7</sup>University of Maryland, College Park, MD, USA

\* now at McGill University, Montreal, QC, Canada

15 *Correspondence to:* Colm Sweeney (colm.sweeney@noaa.gov)

**Abstract.** Accurate estimates of carbon-climate feedbacks require an independent means for evaluating surface flux models at regional scales. Bulk quantities derived from the Arctic Carbon Atmospheric Profiles (Arctic-CAP) project demonstrate the utility of an altitude-integrated enhancement (AIE) diagnostic that leverages background mole fraction values from the middle free troposphere, are agnostic to uncertainties in boundary layer height, and can be derived from model estimates of mole fractions and vertical gradients. To demonstrate the utility of the bulk quantity, six airborne profiling surveys of atmospheric carbon dioxide (CO<sub>2</sub>), methane (CH<sub>4</sub>) and carbon monoxide (CO) throughout Alaska and northwestern Canada between April and November 2017 were completed as part of NASA's Arctic-Boreal Vulnerability Experiment (ABoVE). The Arctic-CAP sampling strategy involved acquiring vertical profiles of CO<sub>2</sub>, CH<sub>4</sub> and CO from the surface to 5 km altitude at 25 sites around the ABoVE domain on a 4- to 6-week time interval. All Arctic-CAP measurements were compared to a global simulation using the Goddard Earth Observing System (GEOS) modeling system. Comparisons of the AIE bulk quantity from aircraft observations and GEOS simulations of atmospheric CO<sub>2</sub>, CH<sub>4</sub> and CO highlight the fidelity of the modeled surface fluxes. The model-data comparison over the ABoVE domain reveals that while current state-of-the-art models and flux estimates are able to capture broadscale spatial and temporal patterns in near-surface CO<sub>2</sub> and CH<sub>4</sub> concentrations, more work is needed to resolve fine-scale flux features that are observed in CO observations.

## 1. Introduction

35 There are many uncertainties to predicting the impact of increased emissions of CO<sub>2</sub> and CH<sub>4</sub> in the atmosphere. Among the most important is the uncertainty we have in our estimate of carbon-climate feedbacks (Arora et al., 2020). Without a better understanding of how changes in temperature, CO<sub>2</sub> itself, water and nutrients are magnifying or reducing the impact of increased emissions of greenhouse

gases (GHG), it will be difficult to use climate models to accurately predict climate change. This uncertainty not only stems from a poor mechanistic understanding of how the biosphere will respond at the smallest scales but also how changes in the landscape drive changes in local environments. The Arctic, in particular, is a region where carbon-climate feedbacks are critical to understand given the vast quantities of carbon sequestered in the permafrost soils of the northern high latitudes (Hugelius et al., 2014), have led to concerns about the potential for significant carbon emissions due to changes in ecosystems, permafrost and large-scale disturbances like fires (Schuur et al., 2015; McGuire et al., 2018; Turetsky et al., 2020). Our understanding of the magnitude and behavior of the carbon system response to these changes is rudimentary (Koven et al., 2015). For instance, release of carbon from the permafrost pool could result in increased emissions of CH<sub>4</sub> from anaerobic degradation; increased emissions of CO<sub>2</sub> from aerobic degradation; increased uptake of carbon due to new availability of nutrients and above-ground ecosystem growth; or an increase in mobilization of carbon through runoff. Alternatively, increases in disturbances such as fires may significantly impact below-ground carbon storage, uptake of CO<sub>2</sub> and emissions of CH<sub>4</sub>, CO, and CO<sub>2</sub>. Limitations in our understanding of the accuracy of modeled fluxes of CO<sub>2</sub>, CO and CH<sub>4</sub> have increased uncertainties in predictions of the magnitude of Arctic carbon-climate feedbacks (e.g., Koven et al., 2011; Schneider von Deimling et al., 2012; Schaefer et al., 2014; Lawrence et al., 2015; Schuur et al., 2015). The lack of observations from which to build and evaluate models of the biosphere is a significant source of the problem and leads to both enhanced uncertainty and reduced fidelity in our model simulations. In general, land- and ocean-atmosphere fluxes from climate models are most commonly evaluated using flux measurements made with eddy covariance or flux chamber techniques (Sasai et al., 2007). While flux measurements of these types are widely available over many ecosystem types, they represent the impact of limited spatial domains that are rarely more than a 1000 m radius around a given site (Schmid, 2002; Gockede et al., 2005) and may be significantly smaller depending on topography, wind direction, boundary layer stability, and measurement approach. Land surface inhomogeneities within these small footprints (Baldocchi et al., 2005) and regional-scale (100-1000 km scales) variability of these ecosystems can lead to significant biases when eddy covariance measurements are scaled up to represent large areas (e.g. Mekonnen et al., 2016). This is especially true in the Arctic where microtopography can result in fluxes varying by orders of magnitude on a scale of 1-100 meters (Johnston et al., 2014). An alternative to the “bottom-up” evaluation approach, which relies on the eddy covariance measurements, is the “top-down” approach, which makes use of atmospheric measurements of species like CO<sub>2</sub>, CH<sub>4</sub> and CO and modeled atmospheric transport patterns to infer the surface fluxes needed to reproduce observed atmospheric concentrations (Pickett-Heaps et al., 2011; Miller et al., 2016; Thompson et al., 2017 are examples in the Arctic) over large regional scales. In a data limited region, this inverse approach generally takes a forward-flux model, or a set of observations that are likely correlated with the flux, as a prior or first guess. The inverse approach then estimates the flux by scaling the prior. While the inverse approach results in a flux estimate that meets the constraint of the trace gas measurements and modeled transport, the variability in surface flux from these analyses cannot be directly attributed to mechanisms such as temperature changes, CO<sub>2</sub> fertilization, nutrient enrichment and water stress and, therefore do not have any predictive capabilities. Also, inverse methods are influenced by errors in atmospheric transport and assumptions about error covariances, which are

80 difficult to characterize (Gourdji et al., 2012; Lauvaux et al., 2012; Mueller et al., 2018; Chatterjee and Michalak, 2013).

In this study, a hybrid approach is taken to evaluate and benchmark the accuracy of current state-of-the-art bottom-up land-surface flux models using a bulk quantity calculated from atmospheric vertical profiles of trace gas mole fractions. The goal is to present an approach to evaluate land-surface flux models that capture complex carbon cycle dynamics over the northern high-latitudes. NASA's Goddard Earth Observing System (GEOS) general circulation model (GCM) is used with a combination of surface flux components for CO<sub>2</sub>, CH<sub>4</sub> and CO to create 4D atmospheric fields; these fields are subsequently evaluated using the altitude-integrated enhancements (AIE) calculated from profiles collected during the Arctic Carbon Atmospheric Profiles (Arctic-CAP) airborne campaign.

85 Both the Arctic-CAP project and the GEOS model runs for the domain are part of NASA's Arctic Boreal Vulnerability Experiment (ABoVE, [www.above.nasa.gov](http://www.above.nasa.gov)), a decade-long research program focused on evaluating the vulnerability and resiliency of the Arctic tundra and boreal ecosystems in western North America (Miller et al., 2019). One of the primary objectives of the ABoVE program is to better understand the major processes driving observed trends in Arctic carbon cycle dynamics, in order to understand how the ecosystem is responding to environmental changes and to characterize the impact of climate feedbacks on greenhouse gas emissions. ABoVE has taken two approaches to better understand critical ecosystem processes vulnerable to change. The first is through ground-based surveys and monitoring sites in representative regions of the ABoVE domain. These multi-year studies provide a backbone for intensive investigations, such as airborne deployments. The Arctic-CAP campaign discussed here was one such airborne deployment that was conducted during the spring-summer-fall of 2017 (Section 2.1). The subsequent analysis described here illustrates how improvements in surface models develop through ground-based surveys, and monitoring sites can be evaluated and tested over larger spatial scales using aircraft profiles (Section 3). This study uses the bulk quantify from Arctic-CAP aircraft profiles to directly evaluate the terrestrial surface flux models of CO<sub>2</sub>, CH<sub>4</sub> and CO. For the sake of demonstration, we rely on one transport model and one flux scenario for each tracer (i.e., CO<sub>2</sub>, CH<sub>4</sub> and CO) to show the utility of the three carbon species to diagnose and identify deficiencies in the land flux models. Ongoing and future studies build upon the results discussed here and further diagnose transport and flux patterns from multiple models based on additional aircraft and ground-based observations throughout the ABoVE domain. This approach demonstrates the value of aircraft profiles.

## 110 2. Methods

### 2.1. Arctic-CAP Flight Planning and Sampling Strategy

Arctic-CAP was designed to measure vertical profiles of atmospheric CO<sub>2</sub>, CH<sub>4</sub> and CO mole fraction to capture the spatial and temporal variability of carbon cycle dynamics (Sweeney et al., 2015; Parazoo et al., 2016) across the ABoVE domain. Six campaigns were performed during 2017: late April – early May, June, July, August, September, and late-October – early November. Arctic-CAP flights surveyed the ABoVE Study Area and were organized around an Alaskan circuit and a Canadian circuit (Fig. 1). The Alaskan circuit covered a region where aircraft measurements were previously made during 2012-2015 by the Carbon in Arctic Reservoirs Vulnerability Experiment (CARVE; Miller et al., 2012), which

120 included the Alaskan Boreal Interior, Brooks Range Tundra and the Alaskan Tundra ecoregions. The Arctic-CAP Alaska circuit was primarily west of Fairbanks, Alaska, and include Galena, Bethel, Unalakleet, Nome and Kotzebue. The northern section of the circuit overflowed Utqiagvik (formerly Barrow), Atkasuk, Deadhorse and the Toolik Lake Research Station – all North Slope tundra sites with long-term measurements of atmospheric CO<sub>2</sub> and CH<sub>4</sub>. The Arctic-CAP Canadian circuit focused on flying over sites in and around the Inuvik and Yellowknife areas in the Canadian Arctic. In the Inuvik region, the aircraft overflowed the Trail Valley Creek and Havipak Creek research sites, and the Daring Lake and Scotty Creek flux tower sites were overflowed on the way to and from the Yellowknife area. The Canadian Circuit expands upon the ecoregions covered in the CARVE missions to include the Boreal Cordillera, Taiga Plain, Taiga Shield and the Southern Arctic Tundra ecoregions. Approximately 25 vertical profiles were acquired during each campaign (Fig 2). The majority of each flight day was spent in the well-mixed boundary layer with 2-4 vertical profiles up to altitudes of 5000 m above sea level (masl). Using missed approaches to get as near to the ground as possible, profiles diagnosed temporal changes in the boundary layer and residual layers above where surface fluxes may have recently (< 3 days) influenced that atmospheric column. During the 2017 season, Arctic-CAP flights were complemented by additional vertical profiles collected in the ABoVE domain by the ASCENDS (Active Sensing of CO<sub>2</sub> Emissions over Nights, Days, & Seasons, <https://www-air.larc.nasa.gov/cgi-bin/ArcView/ascends.2017?MERGE=1>) and ATom (Atmospheric Tomography, Wofsy et al., 2018) campaigns and the NOAA Carbon Cycle Aircraft Program (Karion et al., 2015; Sweeney et al., 2015). The focus of this study will be on the CO<sub>2</sub>, CH<sub>4</sub> and CO data acquired during Arctic-CAP and, in particular, utilizing the profiles acquired during each flight to separate signals from near field surface fluxes from large-scale deviations in a way that is agnostic to model errors due to inaccurate vertical transport.

## 2.2. Aircraft and Payload

145 Arctic-CAP flights were performed with a Mooney Ovation 3 aircraft (tail number N617DH, Scientific Aviation). The Mooney operated at a cruise speed of 170 kts and reached profile altitudes of 5 km (17,000 feet) on each flight, with most legs lasting 4-5 hours and covering an average distance of ~1350 km. The average ascent and descent rates were limited to ~100 m/min to minimize hysteresis in the temperature and relative humidity measurements. The basic research payload flown on all six research missions included continuous in-situ CO<sub>2</sub>, CH<sub>4</sub>, CO, H<sub>2</sub>O, temperature and horizontal winds. The in-situ measurements (Sweeney and McKain, 2019) followed the methodology described in Karion et al. (2013), and wind measurements followed the protocol outlined in Conley et al. (2014). During Arctic-CAP, insitu measurements of CO<sub>2</sub>, CH<sub>4</sub> and CO were made every ~2.4 s and aggregated to 10 s averages for comparison the GEOS 4D fields (latitude, longitude, altitude and time). Sampling at the 10 s resolution reduces the spatial representativeness error between the model grid cell and the aircraft observations.

155 Programmable flask packages (PFPs; Sweeney et al., 2015) provided an independent check of the calibration scale of the continuous *in situ* CO<sub>2</sub>, CH<sub>4</sub> and CO measurements, as well as samples for more than 50 different species including N<sub>2</sub>O, SF<sub>6</sub>, and a variety of hydrocarbons, halocarbons and isotopes of carbon (Sweeney et al., 2020). Carbonyl sulfide measured in the flask samples can be used as a tracer

160 of gross primary productivity (GPP) (Montzka et al., 2007), while ethane, propane and C-13 isotope of CH<sub>4</sub> provide another constraint on the source of the CH<sub>4</sub> emissions. Each flight sampled a single 12-flask package providing a total of ~84 flasks per research mission to better understand the factors controlling local fluxes of CO<sub>2</sub>, CH<sub>4</sub> and CO and the long-range transport of these species from low latitudes.

### 165 2.3. GEOS Earth System Model & Atmospheric CO<sub>2</sub>, CO and CH<sub>4</sub> Modelling

The GEOS (Rienecker et al., 2011; Molod et al., 2015) model is a complex yet flexible modeling system that describes the behavior of the land and atmosphere on a variety of spatial (~12.5-100 km) and temporal (hourly to decadal) scales. GEOS includes both an atmospheric General Circulation Model (GCM) and data assimilation system that have been used to produce the widely-used Modern-  
170 Era Retrospective Analysis for Research and Applications (MERRA) (Rienecker et al., 2011) and MERRA-2 (Bosilovich et al., 2015; Gelaro et al., 2017). The GEOS Forward Processing (GEOS FP) system produces atmospheric analyses and 10-day forecasts in near real-time, which are used to provide forecasting support to NASA field campaigns and satellite instrument teams (e.g. Strode et al., 2018). GEOS has also been used extensively to study atmospheric carbon species (e.g. Allen et al., 2012; Ott et al., 2015; Weir et al., 2020).

The GEOS setup utilized in this work simulates CO<sub>2</sub>, CO and CH<sub>4</sub> simultaneously at nominal 0.5° horizontal resolution, 72 vertical layers (up to ~0.1 hPa) with trace gas output saved every 3-hours. For CO<sub>2</sub>, the surface fluxes consist of 5 different components from a Low-order Flux Inversion (LoFI) package (Weir et al., 2020): 1) net ecosystem exchange (NEE) from the Carnegie Ames Stanford  
180 Approach - Global Fire Emissions Database (CASA-GFED) mode with a parametric adjustment applied to match the atmospheric growth rate (Weir et al., 2020), 2) anthropogenic biofuel burning emissions, i.e., harvested wood product (Van Der Werf et al., 2003), 3) biomass burning emissions derived from the fire radiative power based Quick Fire Emissions Dataset (QFED; Darmenov and Da Silva, 2015) 4) fossil fuel emissions from the Open-source Data Inventory for Anthropogenic CO<sub>2</sub> (ODIAC; Oda and  
185 Maksyutov, 2011), and 5) ocean exchange fluxes based on *in situ* measurements of the partial pressure of CO<sub>2</sub> in sea-water from the Takahashi et al. (2009) dataset but adding back the inter-annual variability and applying a mean pCO<sub>2</sub><sup>sw</sup> growth rate of 1.5 μatm/yr at each point every year. For CO, the emissions include biomass burning emissions from QFED, and climatologies of fossil fuel and biofuel emissions and VOC fields (Duncan et al., 2007; Ott et al., 2010). Finally, the CH<sub>4</sub> flux collection consists of five  
190 components: 1) wetland emissions from the process-based ecosystem model LPJ-*wsl* (Lund-Potsdam-Jena model, WSL version - Poulter et al., 2011), 2) biomass burning emissions from the QFED, 3) industrial and fossil fuel emissions from the Emissions Database for Global Atmospheric Research (EDGAR v4.3.2, Janssens-Maenhout et al., 2017; Crippa et al., 2018), 4) agricultural emissions from EDGAR v4.3.2 and 5) anthropogenic biofuel burning emissions from EDGAR v4.3.2. Note that since  
195 the EDGAR v4.3.2 emissions record ends in 2012, the same set of values from 2012 were used for the year 2017. As shown later, this is not a bad assumption considering that for the majority of the ABoVE domain, the most critical CH<sub>4</sub> emissions are from the wetlands sector. On the other hand, care was taken to use a version of the LPJ-*wsl* model that includes a state-of-the-art hydrology subroutine (TOPMODEL) to determine wetland area and its inter- and intra-annual dynamics (Zhang et al., 2016),  
200 a permafrost and dynamic snow model (Wania et al., 2009) with explicit representation of the effects of

snow and freeze/thaw cycles on soil temperature and moisture, and thus the CH<sub>4</sub> emissions. Table 1 provides a summary of the flux components, their specifications and associated references.

#### 2.4. AIE calculation

205 As will be explained in the following results section the surface fluxes of CO<sub>2</sub>, CH<sub>4</sub> and CO in GEOS is compared to aircraft observations by first subtracting the average daily free tropospheric value (>3000 m for CO<sub>2</sub> and CH<sub>4</sub> and >4000 m for CO, X<sub>FT</sub>) from each measurement below 3000 m and comparing that to the altitude integrated sum

$$\Delta X = \int_{z=ground}^{z=3000} ((X - X_{FT})/n_{BL}) ndz \quad \text{Eq. 1}$$

210 where  $\Delta X$  is altitude-integrated sum of the mole fraction of species X minus X<sub>FT</sub> divided by the n<sub>BL</sub> where  $n_{BL} = \int_{z=ground}^{z=3000} n dz$  and n is the atmospheric number density. It is assumed that the mole fraction of each trace gas species measured at the lowest point in each profile is constant to the ground level. Ground level altitude is taken from USGS (USGS, 2017). Thus, the AIE is equivalent to average enhancement in the boundary layer after accounting for altitude changes in number density.

215

**Table 1. Components of fluxes for simulation of atmospheric concentrations of CO<sub>2</sub>, CO and CH<sub>4</sub> in GEOS. Flux components that are the primary drivers of observed signals within our study domain are distinguished with italics.**

Flux type	Used in simulation of	Inventory / Process-based model name	Reference
Fossil fuel	CO <sub>2</sub>	ODIAC	Oda and Maksyutov, 2011
Biofuel	CO <sub>2</sub>	CASA-GFED3	Van Der Werf et al., 2003
<i>NEE</i>	CO <sub>2</sub>	LoFI CASA	Weir et al., 2020
Ocean	CO <sub>2</sub>	LoFI Takahashi	Weir et al., 2020
Biomass Burning / Fires	CO <sub>2</sub> , CO,	QFED	Darmenov and Da Silva, 2015
Fossil fuels & biofuels	CO	Climatology	Duncan et al., 2007
VOC	CO	GMI climatology	Duncan et al., 2007
<i>Wetlands</i>	CH <sub>4</sub>	LPJ-wsl	Poulter et al., 2011, Zhang et al.,
Agriculture and waste	CH <sub>4</sub>	EDGAR v4.3.2	Crippa et al., 2018
Biofuels	CH <sub>4</sub>	EDGAR v4.3.2	Crippa et al., 2018
Industrial and fossil fuel	CH <sub>4</sub>	EDGAR v4.3.2	Crippa et al., 2018

220 **Table 2. GEOS CO<sub>2</sub> Flux Estimates (PgC yr<sup>-1</sup>) for 2017. Flux emissions are specified for (a) the natural land sink component, which includes the sum of *NEE* and biomass burning, and (b) all anthropogenic source components, which include fossil fuel and biofuel burning.**

ABOVE Domain		pan-Arctic (>48 N)		Global	
Land Sink	Fuel Sources	Land Sink	Fuel Sources	Land Sink	Fuel Sources
-0.32	0.11	-1.84	1.37	-3.28	11.08

225 We have assessed global and pan-Arctic budgets (Tables 2 and 3) and compared against existing studies and estimates to establish the fidelity of the model fluxes for large-scale assessments. CO<sub>2</sub> flux estimates indicate that the ABOVE domain is a 0.32 PgC sink for our study year, 2017. This represents ~17% of the calculated pan-Arctic terrestrial carbon sink, which is consistent with the fraction of the land area > 48N represented by the ABOVE domain (~16%). Perhaps more significantly, the 1.84 PgC pan-Arctic sink represents 56% of the global sink for 2017. We attribute this large uptake to the vast boreal forests > 48 N, particularly in Siberia (Sasakawa et al., 2013), where the contemporary Arctic tundra is thought to be nearly carbon neutral with uncertainties allowing for a small to moderate sink or a small source (McGuire et al., 2016). These findings are also consistent with Wunch et al. (2013) who used GOSAT satellite data and TCCON ground-based column measurements to determine that interannual variability in Northern Hemisphere CO<sub>2</sub> uptake was dominated by changes in the boreal forest. More recent studies, such as Welp et al. (2016) and Commane et al. (2017) have also used atmospheric inversions to highlight that >90% of the carbon sink in the northern high latitudes reside in the boreal forests. Our simple forward model simulations and the Arctic-CAP data provide a unique opportunity to assess the validity of these previous findings over the ABOVE domain. Sub-regional flux estimates within the ABOVE domain are part of ongoing investigations and will be captured in future studies.

230

235

240 **Table 3. GEOS CH<sub>4</sub> Flux Estimates (TgCH<sub>4</sub> yr<sup>-1</sup>) for 2017. CH<sub>4</sub> flux emissions are specified for (a) the wetland component, and (b) all source components, which include wetlands, industrial and fossil fuel, agriculture and waste, biomass burning, biofuel burning and other natural emissions.**

ABoVE Domain		pan-Arctic (>48 N)		Global	
Wetland	All Sources	Wetland	All Sources	Wetland	All Sources
9.01	11.64	21.74	52.03	187.39	536.01

245 Examination of the specified CH<sub>4</sub> flux estimates for the ABoVE domain (Table 4) reveal a remarkable result: 78% of the emissions, 9.01 TgCH<sub>4</sub> yr<sup>-1</sup>, come from wetlands. Furthermore, ABoVE wetlands emissions account for 41% of pan-Arctic CH<sub>4</sub> wetland emissions. Both results suggest a disproportionately large contribution of North American wetlands to the regional CH<sub>4</sub> budget. Placing this in a larger context, the 52 TgCH<sub>4</sub> yr<sup>-1</sup> from all pan-Arctic emissions account for only about 10% of the global emissions. Our pan-Arctic CH<sub>4</sub> emissions estimate of 52 TgCH<sub>4</sub> yr<sup>-1</sup> is only 60% of the 82-84 TgCH<sub>4</sub> yr<sup>-1</sup> determined by Thompson et al. (2017) for latitudes > 50N and the period 2005-2013. The reasons for this large discrepancy are unclear, particularly since the Thompson et al. (2017) study derived their estimate from an inversion of atmospheric CH<sub>4</sub> observations; previously, such top-down estimates have tended to be lower than most forward model emissions estimates. Subtracting the 11 TgCH<sub>4</sub> yr<sup>-1</sup> we estimate for the ABoVE domain from our pan-Arctic value leaves 41 TgCH<sub>4</sub> yr<sup>-1</sup> for the remainder of the pan-Arctic. Future work with additional observations and model simulations will help us understand how specific sectors in the ABoVE domain can better capture the complexity of pan-Arctic CH<sub>4</sub> emissions. Our overall model value of 536 TgCH<sub>4</sub> yr<sup>-1</sup> for global CH<sub>4</sub> emissions in 2017 falls just outside the range of annual emissions estimates for the decade 2008-2017 (Saunois et al., 2019). This discrepancy is primarily due to the fact that we are looking at different time periods and, unlike Saunois et al. (2019), we do not extrapolate the EDGARv4.3.2 dataset using the extended FAO-CH<sub>4</sub> emissions and/or British Petroleum statistical review of fossil fuel production and consumption (see Equation 1 in Saunois et al., 2019); instead, we adopt a much simpler approach of repeating the EDGARv4.3.2 from 2012 for the year 2017. Contrary to the emissions from the coal, oil and gas sector, our wetland methane flux emissions are obtained from the LPJ-*wsl* model (Table 1). LPJ-*wsl* is one of the prognostic models that provide wetland emission estimates to the global methane budget (Table 2 in Saunois et al., 2019). It is not surprising then that our global wetland CH<sub>4</sub> emission estimates for 2017 is in line with both the bottom-up (100-183 TgCH<sub>4</sub> yr<sup>-1</sup>) and top-down (155-217 Tg CH<sub>4</sub> yr<sup>-1</sup>) estimates used in the global methane budget estimate.

### 3. Results and Discussion

#### 3.1. Analysis of Profiles

270 **Table 4. Arctic-CAP 2017 campaign summary**

Campaign	Start (DOY)	End (DOY)
Apr/May	116	124
June	157	170



July	190	202
August	229	242
September	251	271
Oct/Nov	291	310

Vertical profiles of CO<sub>2</sub>, CH<sub>4</sub> and CO were acquired during 56 flights over the six Arctic-CAP campaigns from late April (day of year (DOY) 116) through early November (DOY 310) 2017 (Table 4). Figure 4 presents the composite vertical profile data for each campaign. The monthly composite CO<sub>2</sub>, CH<sub>4</sub> and CO vertical profiles capture the expected variations in the seasonal cycle. The composite profiles also show more variability in the boundary layer (altitudes < 3000 masl) within each month and across months than in the free troposphere for CO<sub>2</sub> and CH<sub>4</sub> (altitudes > 3000 masl). Unlike CO<sub>2</sub> and CH<sub>4</sub>, CO variability in the free troposphere is significantly greater in July and October than the boundary layer showing either long-range transport of CO or CO injected high (>3000 masl) into the troposphere by local wildfires.

A clearer picture of the vertical gradients between the free troposphere and the boundary layer can be seen by subtracting free tropospheric means from measurements below 3000 masl. The CO<sub>2</sub> gradients between the measurements below 3000 masl and average daily free troposphere values show a drawdown in the boundary layer for most of the profiles starting in June and lasting until the end of the September campaign (Fig. 5). The drawdown signal in CO<sub>2</sub> over the Northern Alaska Tundra (often referred to as the “North Slope”) was most pronounced in mid-July and continued through the September campaign. The CO<sub>2</sub> drawdown in the more southerly regions of the Boreal Cordillera and Alaskan Boreal Interior peaked in August. By the October campaign many regions were showing significant enhancements in the boundary layer CO<sub>2</sub> mole fraction relative to the free troposphere. On the other hand, for both CH<sub>4</sub> and CO, significant enhancements were observed from June through early November. Methane enhancements over the Northern Alaska Tundra were observed from July onward, consistent with patterns observed at the long-term surface monitoring station in Utqiagvik (Sweeney et al., 2016). Similarly, boundary layer CO<sub>2</sub> and CH<sub>4</sub> are both most enhanced in September and October on the North Alaska Tundra. Due to the high variability in CO above 3000 masl during July and October (Fig. 4), it is more difficult to use this approach to derive CO enhancements from surface fluxes. To avoid the impact of fire-based CO that has been injected into the free troposphere, the mean background value is taken from measurements above 4000 masl. This analysis shows that Canadian Taiga and Alaskan Boreal Interior are the predominant sources of boundary layer CO emissions reflecting fires in these regions at that time. It should be noted that large enhancement values for CO<sub>2</sub>, CH<sub>4</sub> and CO were observed with the Alaskan Boreal Interior, which were the result of samples taken in the early morning (10:00 local time) before the boundary layer had fully developed (typically around 11:00-12:00 local time). This trapping of night-time emissions results in significant enhancements that quickly taper off with altitude. These measurements were typically taken during the first profile out of Fairbanks where the majority of the Arctic-CAP flights originated.

### 3.2. Model Data Comparisons

Aircraft profiles that measure the gradient from the boundary layer into the free troposphere are particularly useful for evaluating atmospheric models and for separating errors and uncertainties related to atmospheric vertical transport and surface flux model simulations. This is demonstrated by

comparing surface flux models for CO<sub>2</sub>, CH<sub>4</sub>, and CO using a single GCM to evaluate the land surface flux model.

### 310 3.2.1. Point by Point Comparison

In the GEOS model run used for these comparisons, an effort was made to match the global atmospheric burdens of CO<sub>2</sub>, CH<sub>4</sub> and CO; however, given the uncertainties in the sources and sinks of these trace gases and in the representation of long-range and local atmospheric transport, it is not uncommon to have mean offsets between the observed and the modeled mole fractions. To evaluate surface fluxes in the ABoVE domain, it is important to consider both the impact of regional-scale fluxes and long-range transport processes that control the mole fractions of CO<sub>2</sub>, CH<sub>4</sub> and CO throughout the ABoVE domain. A time series comparison of the modeled and the observed CO<sub>2</sub>, CH<sub>4</sub> and CO mole fractions (Fig. 6) suggests that gross features of the seasonal cycles are matched, although some significant differences require detailed analysis by considering different elements of each vertical profile.

### 3.2.2. Free Troposphere Comparisons

As demonstrated from the analysis of the boundary layer enhancements (Fig. 6) observed during Arctic-CAP, it is useful to subtract the average free tropospheric mole fraction from each profile to better understand the local influences within a particular profile. Differences in the mean free tropospheric values, however, can be a valuable indicator of how large-scale biases in the model influence point-to-point comparisons.

In the case of CO<sub>2</sub>, the mean daily CO<sub>2</sub> mole fraction in the observed free troposphere is increasing faster than modeled values over the course of 6 research missions. The largest offset exceeds a mean value of ~2 ppm (observed – modeled) during the September campaign (Fig. 7). Based on the available model runs, it is difficult to diagnose what causes this offset, although a few hypotheses can be put forward. Given the decreasing latitudinal gradient for CO<sub>2</sub> in the free troposphere at this time of year, the offset could be explained by sluggish meridional transport in the model. Alternatively, exaggerated biological uptake in the model in regions outside the study area could be pulling down the CO<sub>2</sub> in modeled free troposphere more rapidly than the drawdown observed over the ABoVE domain.

Likewise, measured CH<sub>4</sub> increases faster than modeled CH<sub>4</sub> over the course of the campaign. Given the decreasing meridional gradient for CH<sub>4</sub> that exists during the summer months, sluggish transport could explain the difference between model and observations. Alternatively, modeled June-July-August emissions of CH<sub>4</sub> in areas contained by the ABoVE domain could be underestimated, leading to slower increase in modeled free tropospheric CH<sub>4</sub>.

Finally, the difference between modeled and observed mole fractions of CO in the free troposphere is mainly driven by inaccuracies in the modeled CO from fire plumes both within and outside the ABoVE domain. Figures 4, 6 and 7 show observations of large CO enhancements above 4000 masl during the July, August and October/November campaigns. Given the large excursions in the free tropospheric CO between different profiles, local fires were likely responsible for these enhancements. Accurately simulating the injection height of fire plumes is challenging (Freitas et al., 2007; Strode et al., 2018).

The GEOS model distributes biomass burning emissions throughout the planetary boundary layer (PBL) to represent injection above the surface layer, but this method can result in underestimated local emissions for fire plumes detraining in the free troposphere. In regions remote to the ABoVE domain, emissions can be mixed and lofted by large-scale weather systems, which may explain why the model performs better in simulating long-range CO plume transport than it does in capturing the CO enhancements from local fires. The observation-model mismatch is likely compounded by the inability of the model to accurately simulate the subgrid-scale vertical mixing necessary for capturing vertical profiles for local sources.

### 3.2.3. Boundary Layer Comparisons

Accurately modeling boundary layer mole fractions of CO<sub>2</sub>, CH<sub>4</sub> and CO depends on an accurate representation of two key factors. First, there is a need to accurately model the local surface-atmosphere flux and second there is a need to correctly model the physical evolution of the PBL, as well as horizontal transport and vertical mixing out of the PBL into the free troposphere. GCMs have limited horizontal and vertical resolution and require parameterizations to predict both the rate of change and the absolute value of the PBL height over the course of the day. Errors in PBL mixing directly impact the tracer mole fraction estimate. Overestimation of the PBL height causes an artificial dilution of the impact of surface flux. Conversely, underestimation of the PBL height results in amplification of the impact of a surface flux on the simulated PBL mole fraction. Additionally, GCMs typically simulate large-scale horizontal gradients more accurately than PBL height unless there are large topographic changes that occur on horizontal scales less than the model resolution (for GEOS, 0.5 degree). This is because such large-scale patterns are generally well-constrained by the millions of in situ and satellite observations incorporated into meteorological analyses while PBL mixing is represented by highly simplified parameterizations

The three carbon species that we investigate in this study provide different diagnostic information about the model transport and flux specifications. In the case of a gas like CO that often comes from a specific point source in the Arctic, accurate placement of the emissions, both in the horizontal and the vertical, and the modeled wind direction are critical factors. The ABoVE domain is made up of large expanses of forest and tundra in which CO<sub>2</sub> fluxes are more uniformly distributed, making the transport accuracy of individual plumes a less critical factor for simulating CO<sub>2</sub>. Accurately estimating CH<sub>4</sub> mole fractions may be more sensitive to horizontal transport in the PBL if CH<sub>4</sub> emissions are dominated by specific features such as lakes or wetlands, or anthropogenic point sources from oil and gas production such as those observed on the North Slope (Floerchinger et al., 2019). However, we observed consistent PBL CH<sub>4</sub> enhancements throughout each campaign (Fig. 5), suggesting a spatial homogeneity in CH<sub>4</sub> emissions rather than emissions from specific point sources.

### 3.3. Altitude-integrated Enhancements (AIEs)

While individual mole fraction measurements are challenging to reproduce given errors in both modeled surface fluxes and transport, the vertical profile provides a unique opportunity for removing significant uncertainties in transport in order to better assess the surface flux model of a specific long-lived tracer. Assuming that horizontal transport is a relatively small source of bias and the upper part of the free

385 troposphere (>3000 masl) is largely unaffected by local processes, it is possible to use the information  
in the vertical profile to reduce the effects of vertical transport. This can be estimated by vertically  
integrating the net change in the PBL due to a surface flux from the surface to a specific altitude that is  
well above the boundary layer. For this study, almost all the enhancements for CO<sub>2</sub> and CH<sub>4</sub> were  
390 observed below 3000 masl.  
By subtracting the average free tropospheric (FT) values in both the model and the measurements and  
averaging the resulting enhancements or depletions for each profile mapped on equal altitude bins from  
surface to 3000 masl (Eq. 1), we quantify a total enhancement (AIE) resulting from the surface flux  
(Fig. 8). The resulting measured and modeled AIE show good correlations for CO<sub>2</sub> and CH<sub>4</sub> but the CO  
correlations are not as promising.  
395 The average measured enhancement in CO<sub>2</sub> and CH<sub>4</sub> below 3000 masl is correlated with the forward  
model such that more than 50% and 36%, respectively, of the observed variability is captured by the  
model (Fig. 8). The average CO enhancements in the lower 3000 masl is captured by the model with  
lesser accuracy – in fact, the model only captures 26% of the observed variability along with a  
significant bias throughout the growing season.

### 400 3.3.1. CO<sub>2</sub> AIE

To understand the true value of the aircraft profile in evaluating the ability of the surface flux model to  
reproduce observed fluxes over large regional expanses, it is useful to rigorously compare the  
differences between modeled and observed near-surface enhancements. The enhancements of CO<sub>2</sub>  
below 3000 masl shown in Fig. 8 for both data and the GEOS model are well correlated. As expected,  
405 during April/May we see very little change in the AIEs below 3000 masl, while June and July and  
August show significant drawdown, followed by enhancements in September and October/November  
(Fig. 6 and 8). The modeled AIEs in the lower 3000 masl reproduce the observations suggesting that the  
surface flux of CO<sub>2</sub> throughout most of the ABoVE domain is accurately modeled by GEOS.  
Despite the overall agreement indicated by aggregated statistics, a closer look shows significant  
410 differences in observed and modeled CO<sub>2</sub> enhancements for many individual flight days (Fig. 9).  
Inspection of individual profiles (Fig. 10) reveal that in some cases the model is not capturing near-  
ground stratification observed in the river valleys of the interior parts of the ABoVE domain. This is not  
surprising given that the observations have a much higher vertical resolution than the model's vertical  
resolution, which is ~100m in the PBL. Consequently, the observed mole fraction values are much  
415 higher than the model estimates because the model is not able to capture the stratification. However, the  
overall modeled vertical gradients in CO<sub>2</sub> match the observations suggesting that the large-scale vertical  
transport of emissions is accurately simulated above ~1000 masl. As an example, the set of profiles  
from July 10 (Fig. 10) demonstrates that, although infrequent, high PBL heights and emissions from  
fires (as indicated by large (>400 ppb) enhancements in CO) add some uncertainty to the AIE values.  
420 Both of these factors impact the mean free tropospheric correction and altitude of integration that we  
have chosen to accurately capture the total CO<sub>2</sub> enhancement from the surface fluxes.

### 3.3.2. CH<sub>4</sub> AIE

Although the correlation between the observed and modeled AIEs of CH<sub>4</sub> is significant, they are not as good as they are for CO<sub>2</sub>. In particular, we see some clear biases in the seasonality where the  
425 enhancements in the early part of the season are underestimated by the model while the enhancements  
in the later part of the season are overestimated. This is demonstrated both by the comparisons of AIEs  
(Fig. 8) and of mole fraction enhancements below 3000 masl (Fig. 9) where the mean difference  
(observed – modeled) switches from positive to negative over the course of the study period. The  
430 Arctic-CAP profile observations provide a critical point of comparison to which future surface flux  
models of CH<sub>4</sub> can be compared, helping to identify areas where process improvements are needed.

### 3.3.3. CO AIE

The comparison of observed and modeled AIEs of CO is less useful because some of the critical  
assumptions made for this comparison are designed to shed light on surface processes affecting CO<sub>2</sub> and  
CH<sub>4</sub>. The biggest limitation in the CO simulation for interpreting vertical profile observations appears to  
435 be in the accuracy of the vertical distribution of CO emissions. While the model shows an increase in  
mole fractions during the July and October/November campaigns, the extreme mole fractions in the  
observations are twice that of the model (Fig. 6). A good example of how the model and the observed  
mole fractions are different can be seen on July 10, 2017 (Fig. 10) during a flight up the Mackenzie  
River in the Northwest Territories of Canada. Here, large enhancements of CO (>400 ppb) are observed  
440 at altitudes between 3000 and 5000 masl while CH<sub>4</sub> and CO<sub>2</sub> boundary layer enhancements are  
observed below 3000 masl in most of the profiles measured that day. The ~100 ppb CO/ppm CO<sub>2</sub> ratio  
and the large CO enhancement not only support the idea that a fire is the source but that the fire is  
nearby (<100 km). Both the magnitude and altitude of the CO enhancement point to a few critical  
445 limitations in the model that was less important for CO<sub>2</sub> and CH<sub>4</sub>. First, most GCMs, including GEOS,  
do not take into account the massive heat source that fires provide to correctly model the injection of  
fire emissions above the boundary layer. Second, the fire radiative power observations used to estimate  
emissions can be obscured by thick clouds or aerosols resulting in the emissions estimates missing some  
fire hotspots. Third, the heterogenous nature of fires as a surface source of CO means that any  
450 inaccuracies in horizontal transport or location of the fire will play a large role in the ability of the  
model to accurately reproduce the observations. Fourth, the lack of diurnal cycle in biomass burning  
emissions from the emission database (QFED; Table 1) may result in ‘temporal aggregation errors’,  
whereby the model simulations may miss the high emission values that coincide with the daytime  
aircraft observations.

### 3.3.4. Model-data mismatch over ecoregions

455 The bulk quantity AIE can be used to evaluate surface flux models with aircraft profiles at the regional-  
scale (Fig. 11). For most regions and times of year, the difference in CO<sub>2</sub> AIEs is not statistically  
significant; however, there are certain regions such as the Northern Tundra of Alaska, where the  
modeled CO<sub>2</sub> AIEs are significantly different and amplify a pattern that is observed over other regions.  
In early spring, the model slightly overestimates observed boundary layer enhancements but a month

460 later the model underestimates drawdown. Figures 6 and 11 suggest that the peak in early-summer  
model drawdown in CO<sub>2</sub> is preceding the observed CO<sub>2</sub> drawdown. The difference between observed  
and modeled enhancements change sign again during the July flight in Northern Tundra Alaska with an  
underestimation of the drawdown. Similar patterns can be observed in the Canadian Boreal Cordillera,  
465 the same period, however, comparisons over the Western Alaska Tundra depict opposite patterns  
(although far more subtle). While the offsets in the fall months are smaller, there is the suggestion that  
the enhancements in the Southern Arctic and Canadian Taiga ecoregions are both underestimated in the  
model. For CH<sub>4</sub>, the seasonal bias (underestimation in the spring and overestimation between July-  
September) in the AIEs between observations and models stands out as the most significant feature. The  
470 notable exceptions are again the Northern Tundra of Alaska and Canadian Boreal Cordillera, where CH<sub>4</sub>  
AIEs in July and at the end of October are significantly underestimated. For reasons explained earlier,  
the CO comparison is less informative. However, if one were to analyze data from the month of  
September, which had no significant influence from fires in the free troposphere, it would suggest that  
the model continues to underestimate the impact of CO emissions across all regions.

### 475 3.3.5. Separating local, region and global vertical gradients

By extracting enhancements below 3000 masl from the observations and the model we have largely  
separated two major sources of biases and uncertainty in a model-data comparison – vertical transport  
and offsets in background mole fraction. However, it should be acknowledged that gradients between  
the boundary layer and free troposphere are not controlled exclusively by local fluxes and that in the  
480 Arctic, in particular, vertical gradients can be controlled by non-local influences. To explore the impact  
of long-range transport Parazoo et al. (2016) performed three simulations to better understand the  
drivers of the vertical gradient over Alaska and found that 48% of the amplitude (April/May-  
July/August) in the seasonal vertical gradient was driven by local fluxes from Alaska while the rest was  
driven by fluxes from the rest of the Arctic (11%) and low latitude (<60N, 41%). For CO<sub>2</sub>, the impact of  
485 long-range transport to the vertical gradient is complicated by the difference in timing of the initial  
drawdown in the spring and the uptick in the fall at low latitudes verses that of high latitudes. The  
earlier drawdown of CO<sub>2</sub> at low latitudes and the transport of that air via the free troposphere to Arctic  
significantly reduces the negative vertical gradient in the Arctic. At the same time, the early uptick of  
CO<sub>2</sub> mole fraction in the Arctic relative to the low latitudes enhances the positive vertical gradient in the  
490 early fall (Parazoo et al., 2016).

To account for the background vertical gradient in CH<sub>4</sub> entering the contiguous US, Baier et al. (2020)  
and Lan et al. (2019) subtracted 12-15 ppt from the vertical gradient to account for a preexisting  
gradient in CH<sub>4</sub> coming onto the continent. Analysis of the background gradient suggests that this  
preexisting vertical gradient is a combination of upstream emissions and wind shear which separates the  
495 origin of the boundary layer air from that of the free troposphere. Large meridional gradients in CH<sub>4</sub>,  
such as those observed in the mid latitudes, will drive depletion of the free troposphere relative to that  
of the boundary layer over the Arctic. Similarly, CO vertical gradients will also be affected by non-local  
fluxes and wind shear between the boundary layer and the free troposphere. In the case of CO and CH<sub>4</sub>  
there is also likely to be a vertical gradient that is influenced by the oxidation of these molecules.

500 However, given the relatively long residence time of these molecules and the low sampling altitude in  
the free troposphere (between 3000 and 5000 masl) of this experiment, this effect is small.  
From this perspective, the preexisting vertical gradient outside the domain of interest illustrates the  
importance of the model accuracy in non-local fluxes and the importance of long-range transport in the  
analysis. One approach ensuring a better boundary conditions is to use a global inversion (e.g.  
505 CarbonTracker (Peters et al., 2007)) to initialize the local region where the prognostic flux model is  
then run to simulate local fields as is done to initialize regional Lagrangian inversion models (e.g. Hu et  
al., 2019).

### 3.3.6. AIEs as a tool for benchmarking fluxes

This comparison of AIEs from Arctic-CAP and GEOS demonstrates one of the many values of the  
510 aircraft profiles as metric for evaluating model performance. In a similar vein, Stephens et al. (2007)  
used the vertical gradient to evaluate the model performance which pointed significant errors both from  
the surface flux models and the vertical transport in the Transcom 3 inversions (Gurney et al., 2002;  
2004). The AIE approach has also been used extensively in the Amazon and Arctic as means of  
optimizing fluxes in an inversion framework. Zhou et al. (2002), Miller et al. (2007) and Gatti et al.  
515 (2010; 2014) have all used some form of AIE from aircraft profiles to estimate surface fluxes of CO<sub>2</sub>  
and CH<sub>4</sub> in the Amazon basin. Similarly, Zhang et al. (2014), Hartery et al. (2018) and Commane et al.  
(2017) use the AIE to produce a set of optimized fluxes CH<sub>4</sub> and CO<sub>2</sub> in the Alaska region. This  
approach to quantifying regional fluxes has significant advantage over other approaches because it less  
dependent on an accurate simulation of vertical transport and boundary layer height as point out in  
520 section 3.2.3. However, even in this instance there is a need to calculate the average influence of the  
boundary layer enhancements and this can change dramatically depending on the accuracy of the  
modelled boundary layer height relative to the integration height of the AIE. In the comparison between  
observed and modelled AIE presented in this study the focus is on benchmarking a given model's  
ability to reproduce the AIE in different regions and seasons to objectively quantify how this model  
525 might do as conditions change as is expected with changing climate. From this perspective the need for  
an accurate simulation of vertical transport largely disappears because the near-field fluxes are not  
being computed but just evaluated. The obvious caveat to this approach is that changing climate will  
bring with it different covariations in temperature, water, radiation and nutrient availability that cannot  
be reproduced over this time and space domain. While this approach does not replace model bench  
530 marking using eddy covariance measurements, it provides an important view of how modelled  
processes reproduce observations over scales of 1-3 days and 10-100s of kms.

## 4. Conclusions

The Arctic-CAP campaign was composed of 6 different research missions from April to November  
2017. It sampled CO<sub>2</sub>, CH<sub>4</sub> and CO vertical profiles from the surface to 5000 masl across the ABoVE  
535 domain in Alaska and Northwestern Canada, covering 6 major Arctic ecoregions. Arctic-CAP airborne  
surveys included large Tundra and Boreal ecosystems that are the likely sources of large changes in the  
seasonal cycle of CO<sub>2</sub> and have been the subject of great speculation about future emissions of CH<sub>4</sub>.

Arctic-CAP's CO<sub>2</sub>, CH<sub>4</sub> and CO profiles provide an excellent basis for evaluating the surface flux models used within state-of-the-art atmospheric transport models, and thus, are an important tool for understanding carbon cycle feedbacks. Comparisons of Arctic-CAP CO<sub>2</sub>, CH<sub>4</sub> and CO observations against GEOS model show the following main results. For CO<sub>2</sub>, the flux model (land and ocean biosphere and fossil fuel) reproduces seasonal and regional depletions and enhancements observed by aircraft profiles after adjusting for small systematic offsets. For CH<sub>4</sub>, the model simulations agree reasonably well with the observed vertical profiles, but the model underestimates CH<sub>4</sub> in the spring and overestimates it in the fall. Modeled North Slope CH<sub>4</sub> is underestimated throughout the measurement period pointing to deficiencies in the wetland flux specifications over this ecoregion. For CO, the comparison between modeled and observed values were confounded by large biomass burning enhancements in the free troposphere that were not captured in the model. Despite these minor shortcomings, the forward model estimates for CO<sub>2</sub> and CH<sub>4</sub> represent a marked improvement in model-data differences compared to those done previously for CARVE (Chang et al., 2014; Commane et al., 2017). Results and the flux budgets demonstrate that model representation of CO<sub>2</sub> and CH<sub>4</sub> for northern high-latitude ecosystems have advanced significantly since the state-of-the-science survey by Fisher et al. (2014). Inversions of the Arctic-CAP data using these fluxes as the prior estimate should further refine the flux estimates and the budget for the ABoVE domain. We note that our comparisons used only GEOS forward model values and slightly different model-data mismatches may be obtained by using a different transport model.

This study highlights the value of collocated airborne CO<sub>2</sub>, CH<sub>4</sub> and CO vertical profiles for quantifying model strengths and weaknesses and for benchmarking fluxes over larger spatial and temporal scales than is offered by EC comparisons. Such evaluation information is essential to improve model characterization of both surface-atmosphere fluxes and to improve our confidence in the accuracy of projections of future conditions. We strongly recommend regular, systematic CO<sub>2</sub>, CH<sub>4</sub> and CO vertical profile observations across the Arctic as an important and cost-effective method to monitor the Arctic for abrupt transformations or potential tipping points in the permafrost-carbon system.

## 5. Data Availability

Arctic-CAP insitu data can be found at <https://doi.org/10.3334/ORNLDAAAC/1658>

## 6. Sample Availability

N/A

## 7. Video supplement

N/A



570 **8. Supplement link**

N/A

**9. Team List**

N/A

**10. Author contributions**

575 CS, KM, CM, AC did experimental design. CS, TN, SW, KM carried out experiment. CS, AC, CM, KM, RB, SW, LS, LH helped with manuscript.

**11. Competing interests**

The authors declare that they have no conflict of interest.

**12. Disclaimer**

580 N/A

**13. Special issue statement**

N/A

**14. Acknowledgements**

585 This research was supported by the NASA Terrestrial Ecology Program award #NNX17AC61A, “Airborne Seasonal Survey of CO<sub>2</sub> and CH<sub>4</sub> Across ABOVE Domain”, as part of the Arctic-Boreal Vulnerability Experiment (ABOVE). A portion of the research presented in this paper was performed at the Jet Propulsion Laboratory, California Institute of Technology, under contract with the National Aeronautics and Space Administration. GEOS model runs and the work of AC was supported by funding from the NASA ROSES-2016 Grant/Cooperative Agreement NNX17AD69A.

590 **15. References**

Allen, M., Erickson, D., Kendall, W., Fu, J., Ott, L., and Pawson, S.: The influence of internal model variability in GEOS-5 on interhemispheric CO<sub>2</sub> exchange, *Journal of Geophysical Research-Atmospheres*, 117, 10.1029/2011jd017059, 2012.

- Arora, V. K., Katavouta, A., Williams, R. G., Jones, C. D., Brovkin, V., Friedlingstein, P., Schwinger, J., Bopp, L., Boucher, O., Cadule, P., Chamberlain, M. A., Christian, J. R., Delire, C., Fisher, R. A., Hajima, T., Ilyina, T., Joetzjer, E., Kawamiya, M., Koven, C. D., Krasting, J. P., Law, R. M., Lawrence, D. M., Lenton, A., Lindsay, K., Pongratz, J., Raddatz, T., Séférian, R., Tachiiri, K., Tjiputra, J. F., Wiltshire, A., Wu, T., and Ziehn, T.: Carbon–concentration and carbon–climate feedbacks in CMIP6 models and their comparison to CMIP5 models, *Biogeosciences*, 17, 4173–4222, 10.5194/bg-17-4173-2020, 2020.
- Baier, B. C., Sweeney, C., Choi, Y., Davis, K. J., DiGangi, J. P., Feng, S., Fried, A., Halliday, H., Higgs, J., Lauvaux, T., Miller, B. R., Montzka, S. A., Newberger, T., Nowak, J. B., Patra, P., Richter, D., Walega, J., and Weibring, P.: Multispecies Assessment of Factors Influencing Regional CO<sub>2</sub> and CH<sub>4</sub> Enhancements During the Winter 2017 ACT-America Campaign, *Journal of Geophysical Research-Atmospheres*, 125, 10.1029/2019jd031339, 2020.
- Baldocchi, D. D., Krebs, T., and Leclerc, M. Y.: "Wet/dry Daisyworld": a conceptual tool for quantifying the spatial scaling of heterogeneous landscapes and its impact on the subgrid variability of energy fluxes, *Tellus Ser. B-Chem. Phys. Meteorol.*, 57, 175–188, 10.1111/j.1600-0889.2005.00149.x, 2005.
- Bosilovich, M. G., Chern, J.-D., Mocko, D., Robertson, F. R., and da Silva, A. M.: Evaluating Observation Influence on Regional Water Budgets in Reanalyses, *J. Clim.*, 28, 3631–3649, 10.1175/jcli-d-14-00623.1, 2015.
- Chang, R. Y. W., Miller, C. E., Dinardo, S. J., Karion, A., Sweeney, C., Daube, B. C., Henderson, J. M., Mountain, M. E., Eluszkiewicz, J., Miller, J. B., Bruhwiler, L. M. P., and Wofsy, S. C.: Methane emissions from Alaska in 2012 from CARVE airborne observations, *Proc. Natl. Acad. Sci. U. S. A.*, 111, 16694–16699, 10.1073/pnas.1412953111, 2014.
- Chou, W. W., Wofsy, S. C., Harriss, R. C., Lin, J. C., Gerbig, C., and Sachse, G. W.: Net fluxes of CO<sub>2</sub> in Amazonia derived from aircraft observations, *Journal of Geophysical Research: Atmospheres*, 107, ACH 4-1-ACH 4-15, <https://doi.org/10.1029/2001JD001295>, 2002.
- Commane, R., Lindaas, J., Benmergui, J., Luus, K. A., Chang, R. Y. W., Daube, B. C., Euskirchen, E. S., Henderson, J. M., Karion, A., Miller, J. B., Miller, S. M., Parazoo, N. C., Randerson, J. T., Sweeney, C., Tans, P., Thoning, K., Veraverbeke, S., Miller, C. E., and Wofsy, S. C.: Carbon dioxide sources from Alaska driven by increasing early winter respiration from Arctic tundra, *Proc. Natl. Acad. Sci. U. S. A.*, 114, 5361–5366, 10.1073/pnas.1618567114, 2017.
- Conley, S. A., Faloon, I. C., Lenschow, D. H., Karion, A., and Sweeney, C.: A Low-Cost System for Measuring Horizontal Winds from Single-Engine Aircraft, *J. Atmos. Ocean. Technol.*, 31, 1312–1320, 10.1175/jtech-d-13-00143.1, 2014.
- Crippa, M., Guizzardi, D., Muntean, M., Schaaf, E., Dentener, F., van Aardenne, J. A., Monni, S., Doering, U., Olivier, J. G. J., Pagliari, V., and Janssens-Maenhout, G.: Gridded emissions of air pollutants for the period 1970–2012 within EDGAR v4.3.2, *Earth Syst. Sci. Data*, 10, 1987–2013, 10.5194/essd-10-1987-2018, 2018.
- Darmenov, A. S., and Da Silva, A. M.: The Quick Fire Emissions Dataset (QFED): Documentation of versions 2.1, 2.2 and 2.4., *NASA Technical Report Series on Global Modeling and Data Assimilation*, 38, 2015.
- Duncan, B. N., Strahan, S. E., Yoshida, Y., Steenrod, S. D., and Livesey, N.: Model study of the cross-tropopause transport of biomass burning pollution, *Atmos. Chem. Phys.*, 7, 3713–3736, 10.5194/acp-7-3713-2007, 2007.
- Fisher, J. B., Sikka, M., Oechel, W. C., Huntzinger, D. N., Melton, J. R., Koven, C. D., Ahlstrom, A., Arain, M. A., Baker, I., Chen, J. M., Ciais, P., Davidson, C., Dietze, M., El-Masri, B., Hayes, D., Huntingford, C., Jain, A. K., Levy, P. E., Lomas, M. R., Poulter, B., Price, D., Sahoo, A. K., Schaefer, K., Tian, H., Tomelleri, E., Verbeeck, H., Viovy, N., Wania, R., Zeng, N., and Miller, C. E.: Carbon cycle uncertainty in the Alaskan Arctic, *Biogeosciences*, 11, 4271–4288, 10.5194/bg-11-4271-2014, 2014.
- Floerchinger, C., McKain, K., Bonin, T., Peischl, J., Biraud, S. C., Miller, C., Ryerson, T. B., Wofsy, S. C., and Sweeney, C.: Methane emissions from oil and gas production on the North Slope of Alaska, *Atmospheric Environment*, 218, 10.1016/j.atmosenv.2019.116985, 2019.
- Freitas, S. R., Longo, K. M., Chatfield, R., Latham, D., Silva Dias, M. A. F., Andreae, M. O., Prins, E., Santos, J. C., Gielow, R., and Carvalho, J. A., Jr.: Including the sub-grid scale plume rise of vegetation fires in low resolution atmospheric transport models, *Atmospheric Chemistry and Physics*, 7, 3385–3398, 10.5194/acp-7-3385-2007, 2007.
- Gatti, L. V., Miller, J. B., D'Amelio, M. T. S., Martinewski, A., Basso, L. S., Gloor, M. E., Wofsy, S., and Tans, P.: Vertical profiles of CO<sub>2</sub> above eastern Amazonia suggest a net carbon flux to the atmosphere and balanced biosphere between 2000 and 2009, *Tellus Ser. B-Chem. Phys. Meteorol.*, 62, 581–594, 10.1111/j.1600-0889.2010.00484.x, 2010.
- Gatti, L. V., Gloor, M., Miller, J. B., Doughty, C. E., Malhi, Y., Domingues, L. G., Basso, L. S., Martinewski, A., Correia, C. S. C., Borges, V. F., Freitas, S., Braz, R., Anderson, L. O., Rocha, H., Grace, J., Phillips, O. L., and Lloyd, J.: Drought

- sensitivity of Amazonian carbon balance revealed by atmospheric measurements, *Nature*, 506, 76-80, 10.1038/nature12957, 2014.
- 645 Gelaro, R., McCarty, W., Suárez, M. J., Todling, R., Molod, A., Takacs, L., Randles, C. A., Darmenov, A., Bosilovich, M. G., Reichle, R., Wargan, K., Coy, L., Cullather, R., Draper, C., Akella, S., Buchard, V., Conaty, A., da Silva, A. M., Gu, W., Kim, G.-K., Koster, R., Lucchesi, R., Merkova, D., Nielsen, J. E., Partyka, G., Pawson, S., Putman, W., Rienecker, M., Schubert, S. D., Sienkiewicz, M., and Zhao, B.: The Modern-Era Retrospective Analysis for Research and Applications, Version 2 (MERRA-2), *J. Clim.*, 30, 5419-5454, 10.1175/JCLI-D-16-0758.1, 2017.
- 650 Gockede, M., Markkanen, T., Mauder, M., Arnold, K., Leps, J. P., and Foken, T.: Validation of footprint models using natural tracer measurements from a field experiment, *Agric. For. Meteorol.*, 135, 314-325, 10.1016/j.agrformet.2005.12.008, 2005.
- Gourdji, S. M., Mueller, K. L., Yadav, V., Huntzinger, D. N., Andrews, A. E., Trudeau, M., Petron, G., Nehrkorn, T., Eluszkiewicz, J., Henderson, J., Wen, D., Lin, J., Fischer, M., Sweeney, C., and Michalak, A. M.: North American CO<sub>2</sub> exchange: inter-comparison of modeled estimates with results from a fine-scale atmospheric inversion, *Biogeosciences*, 9, 457-475, 10.5194/bg-9-457-2012, 2012.
- 655 Gurney, K. R., Law, R. M., Denning, A. S., Rayner, P. J., Baker, D., Bousquet, P., Bruhwiler, L., Chen, Y. H., Ciais, P., Fan, S., Fung, I. Y., Gloor, M., Heimann, M., Higuchi, K., John, J., Maki, T., Maksyutov, S., Masarie, K., Peylin, P., Prather, M., Pak, B. C., Randerson, J., Sarmiento, J., Taguchi, S., Takahashi, T., and Yuen, C. W.: Towards robust regional estimates of CO<sub>2</sub> sources and sinks using atmospheric transport models, *Nature*, 415, 626-630, 2002.
- 660 Gurney, K. R., Law, R. M., Denning, A. S., Rayner, P. J., Pak, B. C., Baker, D., Bousquet, P., Bruhwiler, L., Chen, Y. H., Ciais, P., Fung, I. Y., Heimann, M., John, J., Maki, T., Maksyutov, S., Peylin, P., Prather, M., and Taguchi, S.: Transcom 3 inversion intercomparison: Model mean results for the estimation of seasonal carbon sources and sinks, *Global Biogeochemical Cycles*, 18, 10.1029/2003GB002111, 2004.
- Hartery, S., Commane, R., Lindaas, J., Sweeney, C., Henderson, J., Mountain, M., Steiner, N., McDonald, K., Dinardo, S. J., Miller, C. E., Wofsy, S. C., and Chang, R. Y. W.: Estimating regional-scale methane flux and budgets using CARVE aircraft measurements over Alaska, *Atmos. Chem. Phys.*, 18, 185-202, 10.5194/acp-18-185-2018, 2018.
- 665 Hu, L., Andrews, A. E., Thoning, K. W., Sweeney, C., Miller, J. B., Michalak, A. M., Dlugokencky, E., Tans, P. P., Shiga, Y. P., and Mountain, M.: Enhanced North American carbon uptake associated with El Niño, *Science advances*, 5, eaaw0076, 2019.
- Hugelius, G., Strauss, J., Zubrzycki, S., Harden, J. W., Schuur, E. A. G., Ping, C. L., Schirmermeister, L., Grosse, G., Michaelson, G. J., Koven, C. D., O'Donnell, J. A., Elberling, B., Mishra, U., Camill, P., Yu, Z., Palmtag, J., and Kuhry, P.: Estimated stocks of circumpolar permafrost carbon with quantified uncertainty ranges and identified data gaps, *Biogeosciences*, 11, 6573-6593, 10.5194/bg-11-6573-2014, 2014.
- 670 Janssens-Maenhout, G., Crippa, M., Guizzardi, D., Muntean, M., and Schaaf, E.: Emissions Database for Global Atmospheric Research, version v4.3.2 part I Greenhouse gases (time-series), in: Joint Research Centre (JRC), v4.3.2 ed., European Commission, 2017.
- 675 Karion, A., Sweeney, C., Wolter, S., Newberger, T., Chen, H., Andrews, A., Kofler, J., Neff, D., and Tans, P.: Long-term greenhouse gas measurements from aircraft, *Atmos. Meas. Tech.*, 6, 511-526, 10.5194/amt-6-511-2013, 2013.
- Karion, A., Sweeney, C., Kort, E. A., Shepson, P. B., Brewer, A., Cambaliza, M., Conley, S. A., Davis, K., Deng, A., Hardesty, M., Herndon, S. C., Lauvaux, T., Lavoie, T., Lyon, D., Newberger, T., Petron, G., Rella, C., Smith, M., Wolter, S., Yacovitch, T. I., and Tans, P.: Aircraft-Based Estimate of Total Methane Emissions from the Barnett Shale Region, *Environ. Sci. Technol.*, 49, 8124-8131, 10.1021/acs.est.5b00217, 2015.
- 680 Koven, C. D., Ringeval, B., Friedlingstein, P., Ciais, P., Cadule, P., Khvorostyanov, D., Krinner, G., and Tarnocai, C.: Permafrost carbon-climate feedbacks accelerate global warming, *Proc. Natl. Acad. Sci. U. S. A.*, 108, 14769-14774, 10.1073/pnas.1103910108, 2011.
- 685 Lan, X., Tans, P., Sweeney, C., Andrews, A., Dlugokencky, E., Schwietzke, S., Kofler, J., McKain, K., Thoning, K., and Crotwell, M.: Long-Term Measurements Show Little Evidence for Large Increases in Total US Methane Emissions Over the Past Decade, *Geophysical Research Letters*, 46, 4991-4999, 2019.
- Lauvaux, T., Schuh, A. E., Uliasz, M., Richardson, S., Miles, N., Andrews, A. E., Sweeney, C., Diaz, L. I., Martins, D., Shepson, P. B., and Davis, K. J.: Constraining the CO<sub>2</sub> budget of the corn belt: exploring uncertainties from the assumptions in a mesoscale inverse system, *Atmospheric Chemistry and Physics*, 12, 337-354, 10.5194/acp-12-337-2012, 2012.
- 690

- Lawrence, D. M., Koven, C. D., Swenson, S. C., Riley, W. J., and Slater, A. G.: Permafrost thaw and resulting soil moisture changes regulate projected high-latitude CO<sub>2</sub> and CH<sub>4</sub> emissions, *Environmental Research Letters*, 10, 10.1088/1748-9326/10/9/094011, 2015.
- 695 McGuire, A. D., Koven, C., Lawrence, D. M., Clein, J. S., Xia, J., Beer, C., Burke, E., Chen, G., Chen, X., Delire, C., Jafarov, E., MacDougall, A. H., Marchenko, S., Nicolsky, D., Peng, S., Rinke, A., Saito, K., Zhang, W., Alkama, R., Bohn, T. J., Ciais, P., Decharme, B., Ekici, A., Gouttevin, I., Hajima, T., Hayes, D. J., Ji, D., Krinner, G., Lettenmaier, D. P., Luo, Y., Miller, P. A., Moore, J. C., Romanovsky, V., Schaedel, C., Schaefer, K., Schuur, E. A. G., Smith, B., Sueyoshi, T., and Zhuang, Q.: Variability in the sensitivity among model simulations of permafrost and carbon dynamics in the permafrost region between 1960 and 2009, *Global Biogeochemical Cycles*, 30, 1015-1037, 10.1002/2016gb005405, 2016.
- 700 Mekonnen, Z. A., Grant, R. F., and Schwalm, C.: Sensitivity of modeled NEP to climate forcing and soil at site and regional scales: Implications for upscaling ecosystem models, *Ecological Modelling*, 320, 241-257, <https://doi.org/10.1016/j.ecolmodel.2015.10.004>, 2016.
- Miller, C. E., Dinardo, S. J., Team, C. S., and Ieee: CARVE: The Carbon in Arctic Reservoirs Vulnerability Experiment, in: 2012 Ieee Aerospace Conference, IEEE Aerospace Conference Proceedings, Ieee, New York, 2012.
- 705 Miller, C. E., Griffith, P. C., Goetz, S. J., Hoy, E. E., Pinto, N., McCubbin, I. B., Thorpe, A. K., Hofton, M., Hodkinson, D., Hansen, C., Woods, J., Larson, E., Kasischke, E. S., and Margolis, H. A.: An overview of ABoVE airborne campaign data acquisitions and science opportunities, *Environmental Research Letters*, 14, 10.1088/1748-9326/ab0d44, 2019.
- Miller, J. B., Gatti, L. V., d'Amelio, M. T. S., Crotwell, A. M., Dlugokencky, E. J., Bakwin, P., Artaxo, P., and Tans, P. P.: Airborne measurements indicate large methane emissions from the eastern Amazon basin, *Geophys. Res. Lett.*, 34, 2007.
- 710 Miller, S. M., Commane, R., Melton, J. R., Andrews, A. E., Benmergui, J., Dlugokencky, E. J., Janssens-Maenhout, G., Michalak, A. M., Sweeney, C., and Worthy, D. E. J.: Evaluation of wetland methane emissions across North America using atmospheric data and inverse modeling, *Biogeosciences*, 13, 1329-1339, 10.5194/bg-13-1329-2016, 2016.
- Molod, A., Takacs, L., Suarez, M., and Bacmeister, J.: Development of the GEOS-5 atmospheric general circulation model: evolution from MERRA to MERRA2, *Geoscientific Model Development*, 8, 1339-1356, 10.5194/gmd-8-1339-2015, 2015.
- 715 Mueller, K., Yadav, V., Lopez-Coto, I., Karion, A., Gourdji, S., Martin, C., and Whetstone, J.: Siting Background Towers to Characterize Incoming Air for Urban Greenhouse Gas Estimation: A Case Study in the Washington, DC/Baltimore Area, *Journal of Geophysical Research-Atmospheres*, 123, 2910-2926, 10.1002/2017jd027364, 2018.
- Oda, T., and Maksyutov, S.: A very high-resolution (1 km x 1 km) global fossil fuel CO<sub>2</sub> emission inventory derived using a point source database and satellite observations of nighttime lights, *Atmospheric Chemistry and Physics*, 11, 543-556, 10.5194/acp-11-543-2011, 2011.
- 720 Ott, L., Duncan, B., Pawson, S., Colarco, P., Chin, M., Randles, C., Diehl, T., and Nielsen, E.: Influence of the 2006 Indonesian biomass burning aerosols on tropical dynamics studied with the GEOS-5 AGCM, *Journal of Geophysical Research: Atmospheres*, 115, 10.1029/2009JD013181, 2010.
- Ott, L. E., Pawson, S., Collatz, G. J., Gregg, W. W., Menemenlis, D., Brix, H., Rousseaux, C. S., Bowman, K. W., Liu, J., 725 Eldering, A., Gunson, M. R., and Kawa, S. R.: Assessing the magnitude of CO<sub>2</sub> flux uncertainty in atmospheric CO<sub>2</sub> records using products from NASA's Carbon Monitoring Flux Pilot Project, *Journal of Geophysical Research-Atmospheres*, 120, 734-765, 10.1002/2014jd022411, 2015.
- Parazoo, N. C., Commane, R., Wofsy, S. C., Koven, C. D., Sweeney, C., Lawrence, D. M., Lindaas, J., Chang, R. Y. W., and Miller, C. E.: Detecting regional patterns of changing CO<sub>2</sub> flux in Alaska, *Proc. Natl. Acad. Sci. U. S. A.*, 113, 7733-7738, 10.1073/pnas.1601085113, 2016.
- 730 Peters, W., Jacobson, A., Sweeney, C., Andrews, A., Conway, T., Masarie, K., Miller, J. B., Bruhwiler, L., Petron, G., Hirsch, A., Worthy, D., Werf, G. v. d., Randerson, J. T., Wennberg, P., Krol, M., and Tan, P.: The atmospheric perspective of carbon-dioxide exchange across North America: CarbonTracker, *Proceedings of the National Academy of Sciences of the United States of America (PNAS)*, 2007.
- 735 Pickett-Heaps, C. A., Jacob, D. J., Wecht, K. J., Kort, E. A., Wofsy, S. C., Diskin, G. S., Worthy, D. E. J., Kaplan, J. O., Bey, I., and Drevet, J.: Magnitude and seasonality of wetland methane emissions from the Hudson Bay Lowlands (Canada), *Atmos. Chem. Phys.*, 11, 3773-3779, 10.5194/acp-11-3773-2011, 2011.
- Poulter, B., Ciais, P., Hodson, E., Lischke, H., Maignan, F., Plummer, S., and Zimmermann, N. E.: Plant functional type mapping for earth system models, *Geoscientific Model Development*, 4, 993-1010, 10.5194/gmd-4-993-2011, 2011.

- 740 Rienecker, M. M., Suarez, M. J., Gelaro, R., Todling, R., Bacmeister, J., Liu, E., Bosilovich, M. G., Schubert, S. D., Takacs, L., Kim, G.-K., Bloom, S., Chen, J., Collins, D., Conaty, A., Da Silva, A., Gu, W., Joiner, J., Koster, R. D., Lucchesi, R., Molod, A., Owens, T., Pawson, S., Pegion, P., Redder, C. R., Reichle, R., Robertson, F. R., Ruddick, A. G., Sienkiewicz, M., and Woollen, J.: MERRA: NASA's Modern-Era Retrospective Analysis for Research and Applications, *J. Clim.*, 24, 3624-3648, 10.1175/jcli-d-11-00015.1, 2011.
- 745 Sasai, T., Okamoto, K., Hiyama, T., and Yamaguchi, Y.: Comparing terrestrial carbon fluxes from the scale of a flux tower to the global scale, *Ecological Modelling*, 208, 135-144, <https://doi.org/10.1016/j.ecolmodel.2007.05.014>, 2007.
- Sasakawa, M., Machida, T., Tsuda, N., Arshinov, M., Davydov, D., Fofonov, A., and Krasnov, O.: Aircraft and tower measurements of CO<sub>2</sub> concentration in the planetary boundary layer and the lower free troposphere over southern taiga in West Siberia: Long-term records from 2002 to 2011, *Journal of Geophysical Research: Atmospheres*, 118, 9489-9498, 10.1002/jgrd.50755, 2013.
- 750 Saunio, M., Stavert, A. R., Poulter, B., Bousquet, P., Canadell, J. G., Jackson, R. B., Raymond, P. A., Dlugokencky, E. J., Houweling, S., Patra, P. K., Ciais, P., Arora, V. K., Bastviken, D., Bergamaschi, P., Blake, D. R., Brailsford, G., Bruhwiler, L., Carlson, K. M., Carrol, M., Castaldi, S., Chandra, N., Crevoisier, C., Crill, P. M., Covey, K., Curry, C. L., Etiope, G., Frankenberg, C., Gedney, N., Hegglin, M. I., Höglund-Isaksson, L., Hugelius, G., Ishizawa, M., Ito, A., Janssens-Maenhout, G., Jensen, K. M., Joos, F., Kleinen, T., Krummel, P. B., Langenfelds, R. L., Laruelle, G. G., Liu, L., Machida, T., Maksyutov, S., McDonald, K. C., McNorton, J., Miller, P. A., Melton, J. R., Morino, I., Müller, J., Murgia-Flores, F., Naik, V., Niwa, Y., Noce, S., O'Doherty, S., Parker, R. J., Peng, C., Peng, S., Peters, G. P., Prigent, C., Prinn, R., Ramonet, M., Regnier, P., Riley, W. J., Rosentreter, J. A., Segers, A., Simpson, I. J., Shi, H., Smith, S. J., Steele, L. P., Thornton, B. F., Tian, H., Tohjima, Y., Tubiello, F. N., Tsuruta, A., Viovy, N., Voulgarakis, A., Weber, T. S., van Weele, M., van der Werf, G. R., Weiss, R. F., Worthy, D., Wunch, D., Yin, Y., Yoshida, Y., Zhang, W., Zhang, Z., Zhao, Y., Zheng, B., Zhu, Q., Zhu, Q., and Zhuang, Q.: The Global Methane Budget 2000-2017, *Earth Syst. Sci. Data Discuss.*, 2019, 1-136, 10.5194/essd-2019-128, 2019.
- 755 Schaefer, K., Lantuit, H., Romanovsky, V. E., Schuur, E. A. G., and Witt, R.: The impact of the permafrost carbon feedback on global climate, *Environmental Research Letters*, 9, 10.1088/1748-9326/9/8/085003, 2014.
- Schmid, H. P.: Footprint modeling for vegetation atmosphere exchange studies: a review and perspective, *Agric. For. Meteorol.*, 113, 159-183, 10.1016/s0168-1923(02)00107-7, 2002.
- 760 Schneider von Deimling, T., Meinshausen, M., Levermann, A., Huber, V., Frieler, K., Lawrence, D. M., and Brovkin, V.: Estimating the near-surface permafrost-carbon feedback on global warming, *Biogeosciences*, 9, 649-665, 10.5194/bg-9-649-2012, 2012.
- Schuur, E. A. G., McGuire, A. D., Schaedel, C., Grosse, G., Harden, J. W., Hayes, D. J., Hugelius, G., Koven, C. D., Kuhry, P., Lawrence, D. M., Natali, S. M., Olefeldt, D., Romanovsky, V. E., Schaefer, K., Turetsky, M. R., Treat, C. C., and Vonk, J. E.: Climate change and the permafrost carbon feedback, *Nature*, 520, 171-179, 10.1038/nature14338, 2015.
- 770 Stephens, B. B., Bakwin, P. S., Tans, P. P., Teclaw, R. M., and Baumann, D. D.: Application of a differential fuel-cell analyzer for measuring atmospheric oxygen variations, *J. Atmos. Ocean. Technol.*, 24, 82-94, 10.1175/jtech1959.1, 2007.
- Strode, S. A., Liu, J., Lait, L., Commane, R., Daube, B., Wofsy, S., Conaty, A., Newman, P., and Prather, M.: Forecasting carbon monoxide on a global scale for the ATom-1 aircraft mission: insights from airborne and satellite observations and modeling, *Atmos. Chem. Phys.*, 18, 10955-10971, 10.5194/acp-18-10955-2018, 2018.
- 775 Sweeney, C., Karion, A., Wolter, S., Newberger, T., Guenther, D., Higgs, J. A., Andrews, A. E., Lang, P. M., Neff, D., Dlugokencky, E., Miller, J. B., Montzka, S. A., Miller, B. R., Masarie, K. A., Biraud, S. C., Novelli, P. C., Crotwell, M., Crotwell, A. M., Thoning, K., and Tans, P. P.: Seasonal climatology of CO<sub>2</sub> across North America from aircraft measurements in the NOAA/ESRL Global Greenhouse Gas Reference Network, *Journal of Geophysical Research-Atmospheres*, 120, 5155-5190, 10.1002/2014jd022591, 2015.
- 780 Sweeney, C., Dlugokencky, E., Miller, C. E., Wofsy, S., Karion, A., Dinardo, S., Chang, R. Y. W., Miller, J. B., Bruhwiler, L., Crotwell, A. M., Newberger, T., McKain, K., Stone, R. S., Wolter, S. E., Lang, P. E., and Tans, P.: No significant increase in long-term CH<sub>4</sub> emissions on North Slope of Alaska despite significant increase in air temperature, *Geophysical Research Letters*, 43, 6604-6611, 10.1002/2016gl069292, 2016.
- 785 Sweeney, C., and McKain, K.: ABoVE: Atmospheric Profiles of CO, CO<sub>2</sub> and CH<sub>4</sub> Concentrations from Arctic-CAP, 2017, in, ORNL Distributed Active Archive Center, 2019.
- Sweeney, C., McKain, K., Miller, B. R., and Michel, S. E.: ABoVE: Atmospheric Gas Concentrations from Airborne Flasks, Arctic-CAP, 2017, in, ORNL Distributed Active Archive Center, 2020.

- 790 Takahashi, T., Sutherland, S. C., Wanninkhof, R., Sweeney, C., Feely, R. A., Chipman, D. W., Hales, B., Friederich, G., Chavez, F., Sabine, C., Watson, A., Bakker, D. C. E., Schuster, U., Metzl, N., Yoshikawa-Inoue, H., Ishii, M., Midorikawa, T., Nojiri, Y., Kortzinger, A., Steinhoff, T., Hoppema, M., Olafsson, J., Arnarson, T. S., Tilbrook, B., Johannessen, T., Olsen, A., Bellerby, R., Wong, C. S., Delille, B., Bates, N. R., and de Baar, H. J. W.: Climatological mean and decadal change in surface ocean pCO<sub>2</sub>, and net sea-air CO<sub>2</sub> flux over the global oceans, *Deep-Sea Res. Part II-Top. Stud. Oceanogr.*, 56, 554-577, 10.1016/j.dsr2.2008.12.009, 2009.
- 795 Thompson, R. L., Sasakawa, M., Machida, T., Aalto, T., Worthy, D., Lavric, J. V., Myhre, C. L., and Stohl, A.: Methane fluxes in the high northern latitudes for 2005-2013 estimated using a Bayesian atmospheric inversion, *Atmospheric Chemistry and Physics*, 17, 3553-3572, 10.5194/acp-17-3553-2017, 2017.
- 800 USGS: 1 meter Digital Elevation Models (DEMs) - USGS National Map 3DEP Downloadable Data Collection, in: ScienceBase-Catalogue, edited by: Survey, U. S. G., 2017.
- Van Der Werf, G. R., Randerson, J. T., Collatz, G. J., and Giglio, L.: Carbon emissions from fires in tropical and subtropical ecosystems, *Glob. Change Biol.*, 9, 547-562, 10.1046/j.1365-2486.2003.00604.x, 2003.
- 805 Wania, R., Ross, I., and Prentice, I. C.: Integrating peatlands and permafrost into a dynamic global vegetation model: 1. Evaluation and sensitivity of physical land surface processes, *Global Biogeochemical Cycles*, 23, 10.1029/2008gb003412, 2009.
- Weir, B., Ott, L., Collatz, G., Kawa, S. R., Poulter, B., Chatterjee, A., Oda, T., and Pawson, S.: Calibrating satellite-derived surface carbon fluxes for reanalyses and near real-time monitoring systems, *Atmospheric Chemistry and Physics*, In review, 2020.
- 810 Welp, L. R., Patra, P. K., Rödenbeck, C., Nemani, R., Bi, J., Piper, S. C., and Keeling, R. F.: Increasing summer net CO<sub>2</sub> uptake in high northern ecosystems inferred from atmospheric inversions and comparisons to remote-sensing NDVI, *Atmos. Chem. Phys.*, 16, 9047-9066, 10.5194/acp-16-9047-2016, 2016.
- 815 Wofsy, S. C., Afshar, S., Allen, H. M., Apel, E., Asher, E. C., Barletta, B., Bent, J., Bian, H., Biggs, B. C., Blake, D. R., Blake, N., Bourgeois, I., Brock, C. A., Brune, W. H., Budney, J. W., Bui, T. P., Butler, A., Campuzano-Jost, P., Chang, C. S., Chin, M., Commane, R., Correa, G., Crouse, J. D., Cullis, P. D., Daube, B. C., Day, D. A., Dean-Day, J. M., Dibb, J. E., Digangi, J. P., Diskin, G. S., Dollner, M., Elkins, J. W., Erdesz, F., Fiore, A. M., Flynn, C. M., Froyd, K., Gesler, D. W., Hall, S. R., Hanisco, T. F., Hannun, R. A., Hills, A. J., Hints, E. J., Hoffman, A., Hornbrook, R. S., Huey, L. G., Hughes, S., Jimenez, J. L., Johnson, B. J., Katich, J. M., Keeling, R., Kim, M. J., Kupc, A., Lait, L. R., Lamarque, J. F., Liu, J., McKain, K., McLaughlin, R. J., Meinardi, S., Miller, D. O., Montzka, S. A., Moore, F. L., Morgan, E. J., Murphy, D. M., Murray, L. T., Nault, B. A., Neuman, J. A., Newman, P. A., Nicely, J. M., Pan, X., Paplawsky, W., Peischl, J., Prather, M. J., Price, D. J., Ray, E., Reeves, J. M., Richardson, M., Rollins, A. W., Rosenlof, K. H., Ryerson, T. B., Scheuer, E., Schill, G. P., Schroder, J. C., Schwarz, J. P., St.Clair, J. M., Steenrod, S. D., Stephens, B. B., Strode, S. A., Sweeney, C., Tanner, D., Teng, A. P., Thames, A. B., Thompson, C. R., Ullmann, K., Veres, P. R., Vizenor, N., Wagner, N. L., Watt, A., Weber, R., Weinzierl, B., Wennberg, P., Williamson, C. J., Wilson, J. C., Wolfe, G. M., Woods, C. T., and Zeng, L. H.: ATom: Merged Atmospheric Chemistry, Trace Gases, and Aerosols, in: ORNL Distributed Active Archive Center, 2018.
- 825 Wunch, D., Wennberg, P. O., Messerschmidt, J., Parazoo, N. C., Toon, G. C., Deutscher, N. M., Keppel-Aleks, G., Roehl, C. M., Randerson, J. T., Warneke, T., and Notholt, J.: The covariation of Northern Hemisphere summertime CO<sub>2</sub> with surface temperature in boreal regions, *Atmos. Chem. Phys.*, 13, 9447-9459, 10.5194/acp-13-9447-2013, 2013.
- 830 Zhang, Z., Zimmermann, N. E., Kaplan, J. O., and Poulter, B.: Modeling spatiotemporal dynamics of global wetlands: comprehensive evaluation of a new sub-grid TOPMODEL parameterization and uncertainties, *Biogeosciences*, 13, 1387-1408, 10.5194/bg-13-1387-2016, 2016.





Figure. 1. The Arctic-CAP surveys were designed to sample the Arctic boreal ecosystems of the ABoVE domain. Black text labels represent the six ecoregions covered by this study and white text denote cities and states / provinces. Gray dots depict the locations on which the Arctic-CAP vertical profiles were centered (© Google Earth). Flight track colors represent extent of each (of 7) daily flights (see Figure 2).

840

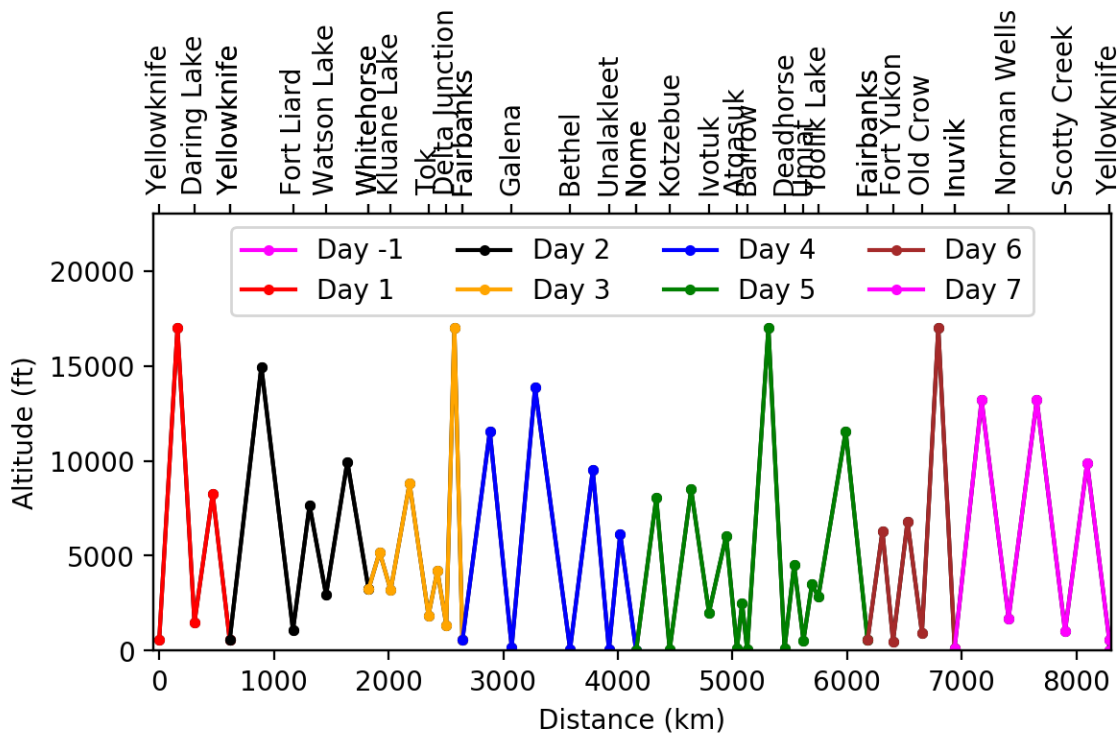
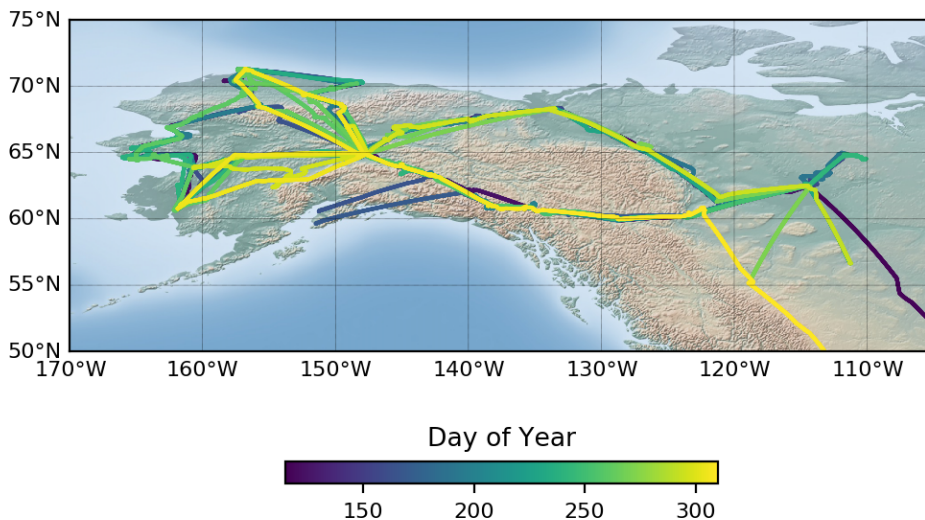
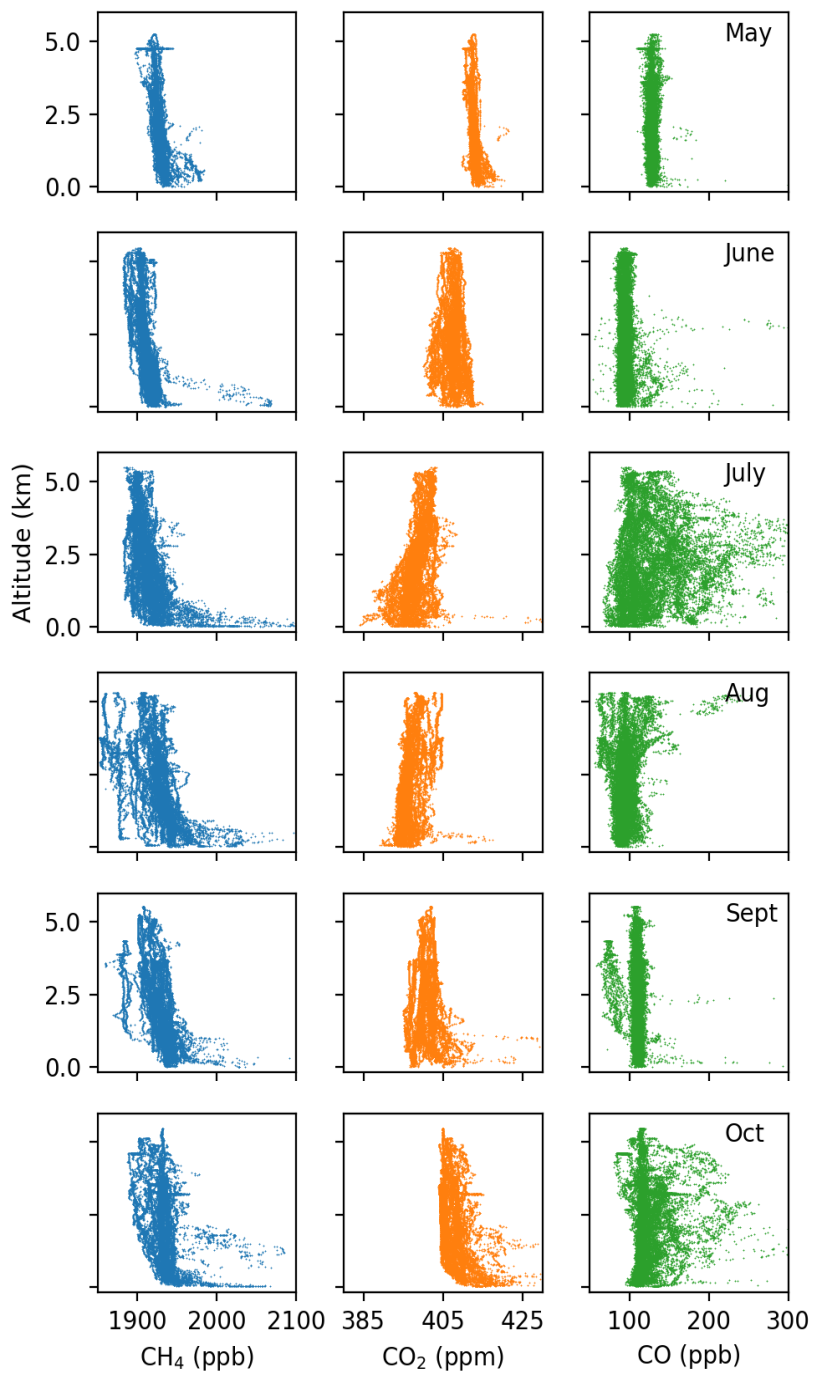


Figure 2. Locations and maximum altitudes of the 25 vertical profiles that were acquired during each Arctic-CAP campaign. The colors match the flight lines illustrated in Fig. 1.

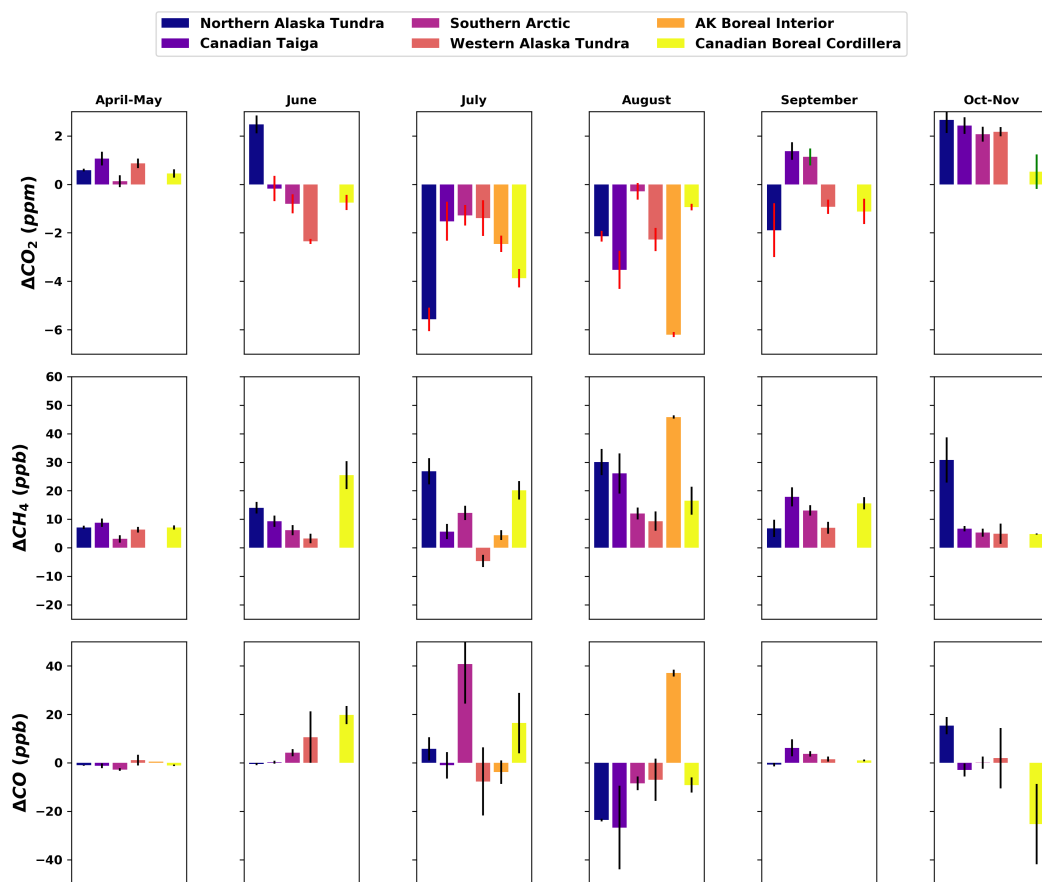


845 Figure 3 Arctic-CAP flight paths colored by day of year (DOY). Later paths are plotted on top, masking flights from earlier in the year along the same routes. Profile locations span 50-75 °N and 105-165 °W and sampled environmental conditions from the spring thaw (~DOY 125) through the early cold season (> DOY 300) (© Google Maps).

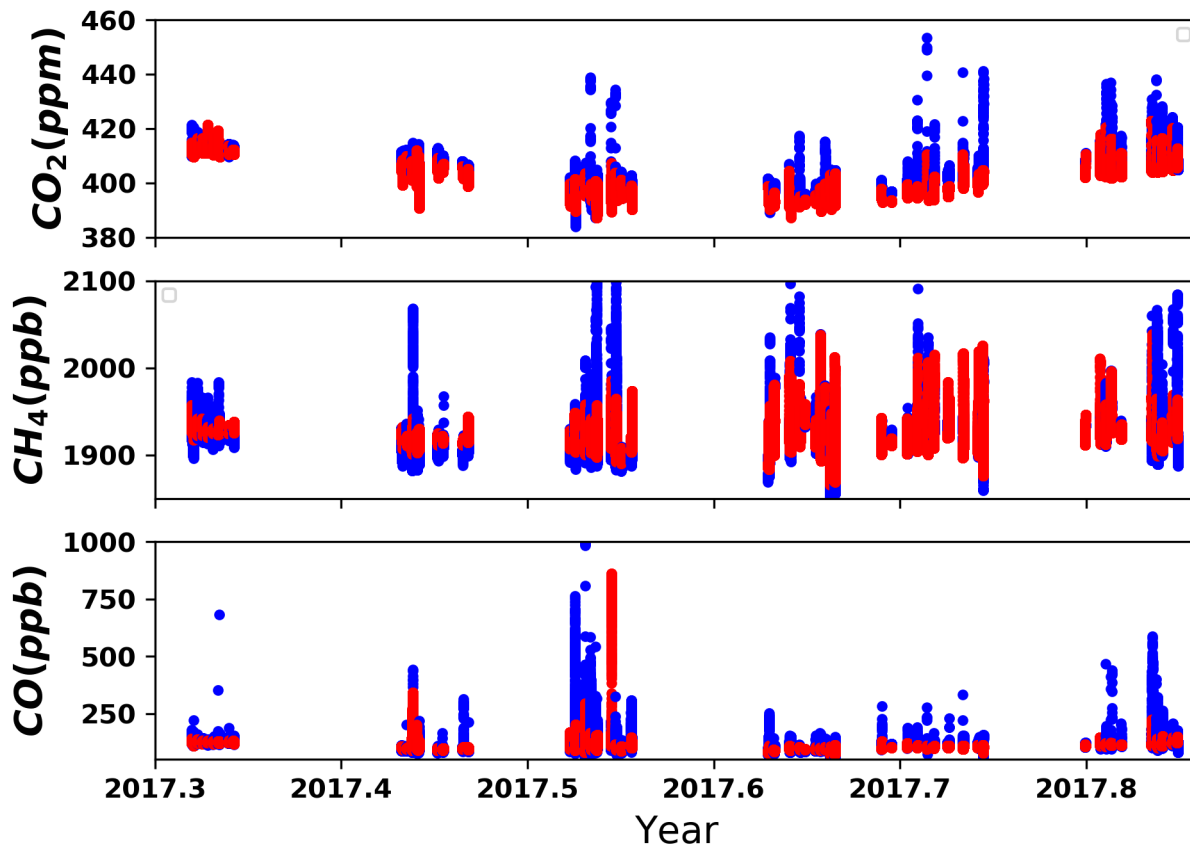




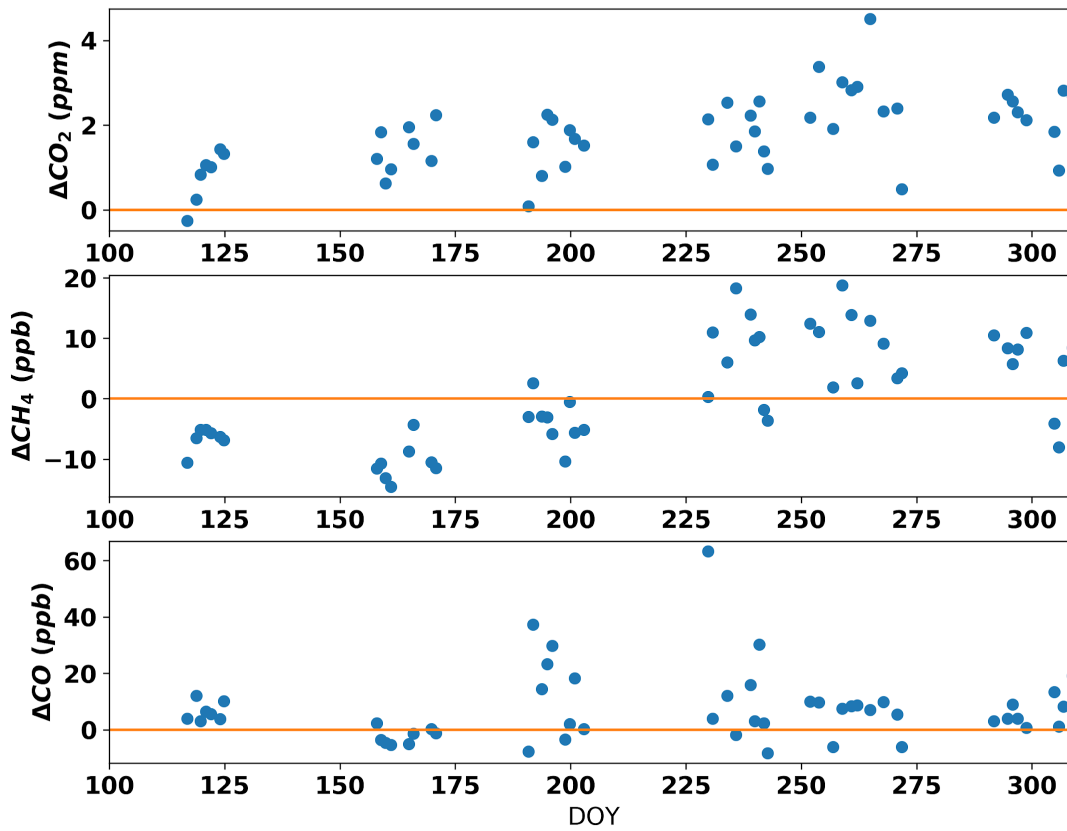
850 **Figure 4. Composite plots of the CH<sub>4</sub> (left column), CO<sub>2</sub> (center column) and CO (right column) measurements acquired during the Arctic-CAP airborne campaign in 2017. Broad seasonal cycle and near surface enhancement (depletions) can be seen as well as the impact of fires to the free tropospheric CO.**



855 **Figure 5. Average gradient between the mean free daily troposphere (> 3000 masl for CO<sub>2</sub> and CH<sub>4</sub> and 4000 masl for CO) and measurements made below 3000 masl during each campaign. Colors refer to the six ecoregions identified in Fig. 1.**



860 Figure 6. Comparisons of GEOS simulated atmospheric CO<sub>2</sub>, CH<sub>4</sub> and CO (red points) versus observed CO<sub>2</sub>, CH<sub>4</sub> and CO (blue points) during the Arctic-CAP 2017 campaign show good agreement across campaigns, although the observed data exhibit larger extremes.



865 **Figure 7.** Difference (observations-model) between mean daily free troposphere (3000-5000 masl for CO<sub>2</sub> and CH<sub>4</sub> and 4000-5000 masl for CO) for GEOS simulated and Arctic-CAP observed mole fractions. The GEOS simulations systematically underestimate the mean CO<sub>2</sub> in all months, while the model overestimates CH<sub>4</sub> before DOY 200 and underestimates CH<sub>4</sub> after DOY 200. Simulated CO observations generally agree with the atmospheric observations, although there are sporadic underestimates likely associated with incorrectly modeled fire plumes.

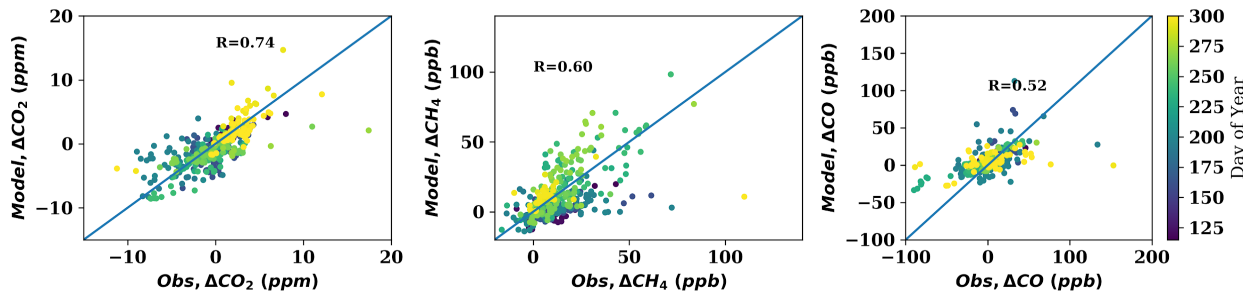


Figure 8. Modelled versus observed average boundary layer enhancements or depletions in  $\text{CO}_2$ ,  $\text{CH}_4$  and  $\text{CO}$  for individual profiles from 3000 masl down to the surface level.

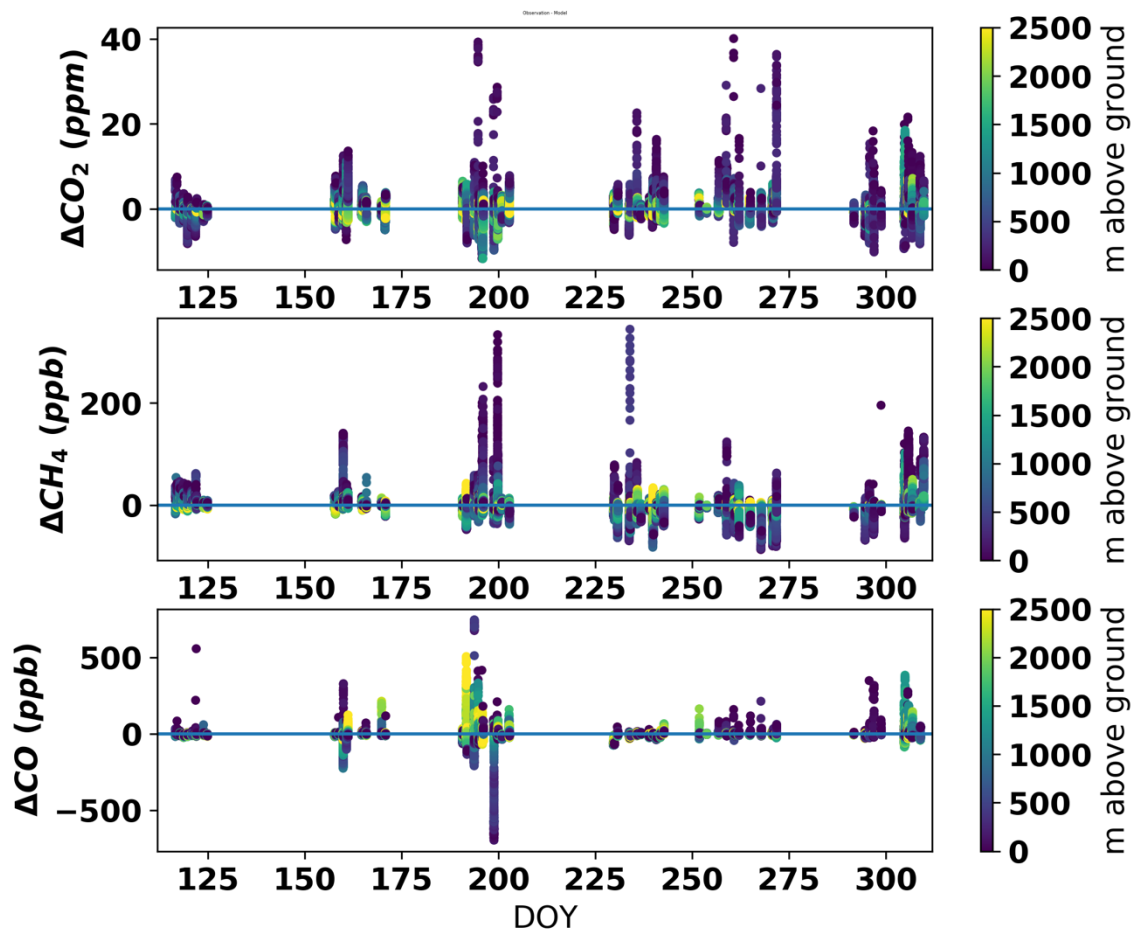
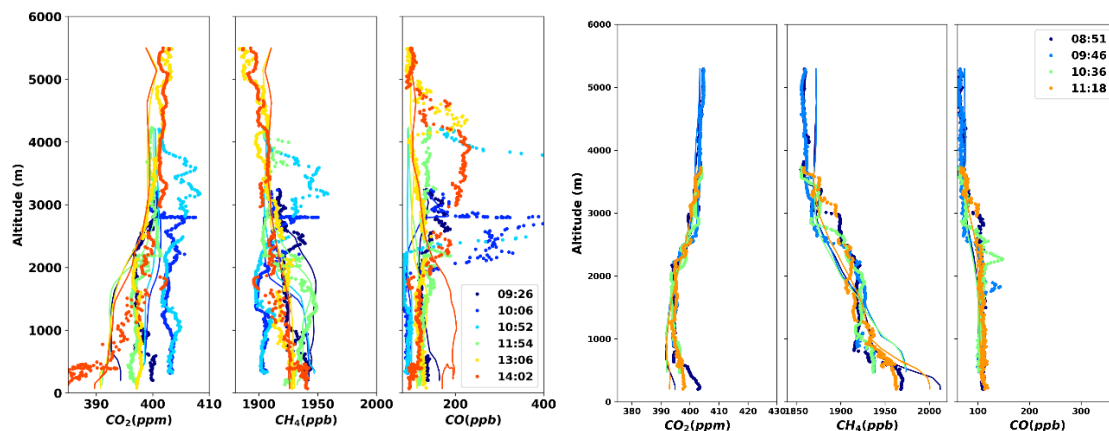
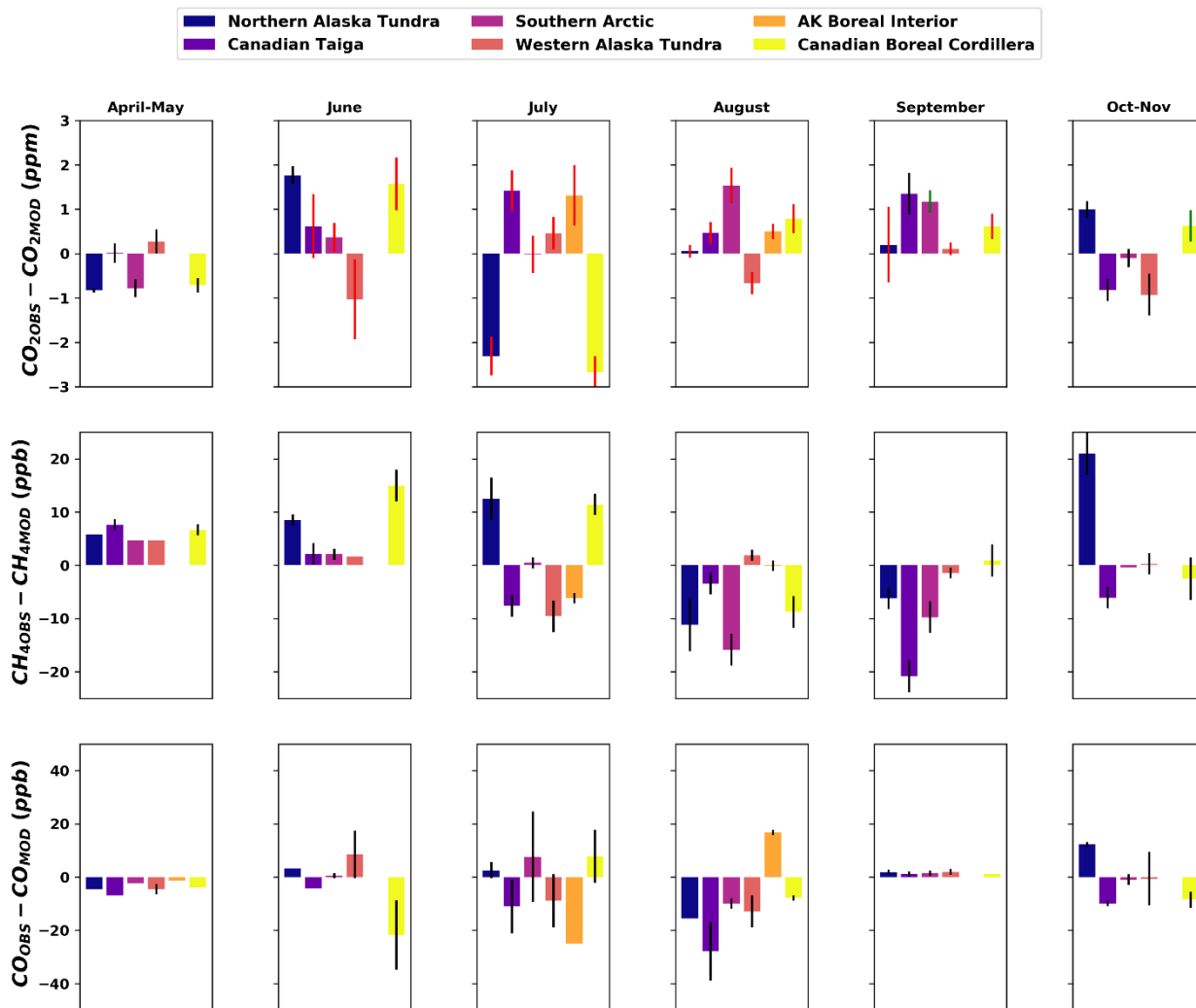


Figure 9. Observation-model differences in mole fractions below 3000 masl. Corrections have been made for observation-model offsets above 3000 masl (Fig. 7). Colors show the altitude of each deviation. Dark blue indicates differences near the surface while yellow indicates differences near 3000 masl.



**Figure 10. Observation (dotted lines) and model estimates (thin lines) of profiles on July 10, 2017 (left) and August 30, 2017 (right) from a transect up the Mackenzie River in the Northwest Territory of Canada. Dotted lines show observations and thin lines show model estimates corresponding to specific times during the transect.**



885 **Figure 11. Average observation–model integrated enhancement differences by ecoregion. Standard deviation of differences for each region are shown with black and red bars. Red (black) bars signify a negative (positive) average enhancement below 3000 meters relative to the daily mean tropospheric value above 3000 masl for  $CO_2$  and  $CH_4$  and above 4000 masl for  $CO$ .**

890